Trend and Bounds for Error Growth in Controlled Lagrangian Particle Tracking

Klementyna Szwaykowska and Fumin Zhang

Abstract

This paper establishes the method of controlled Lagrangian particle tracking (CLPT) to analyse the offsets between physical positions of marine robots in the ocean and simulated positions of controlled particles in an ocean model. The offset, which we term the CLPT error, demonstrates distinguished characteristics not previously seen in drifters and floats that cannot be actively controlled. The CLPT error growth over time is exponential until it reaches a turning point that only depends on the resolution of the ocean model. After this turning point, the error growth slows down significantly to polynomial functions of time. In the ideal case, a theoretical upper threshold on exponential growth of CLPT error can be derived. These characteristics are proved theoretically, verified via simulation, and justified with ocean experimental data. The method of CLPT may be applied to improve the accuracy of ocean circulation models and the performance of navigation algorithms for marine robots.

Index Terms

Autonomous underwater vehicles; stochastic systems; Markov models; model-based control; modeling errors.

I. Introduction

Ocean circulation modeling is an area of active research in physical oceanography. One established method to improve the accuracy of ocean circulation models is the method of Lagrangian particle tracking (LPT) [1], [2]. Unactuated drifting platforms called Lagrangian

School of Electrical and Computer Engineering, Georgia Institute of Technology, 85 Fifth Street NW, Suite 418, Atlanta, GA, 30332. Email: klimka,fumin@ece.gatech.edu

The research work is supported by ONR grants N00014-08-1-1007, N00014-09-1-1074, and N00014-10-10712 (YIP), and NSF grants ECCS-0841195 (CAREER), CNS-0931576, and ECCS-1056253.

floats are deployed in the ocean and are advected freely by the ocean flow. The trajectories of the Lagrangian floats in the ocean are compared with numerically modeled trajectories obtained using the ocean circulation model. It is common practice that Lagrangian floats are idealized as massless Lagrangian particles.

Tracking of particles in ocean flows has a wide range of applications, and there have been numerous attempts to accurately predict distributions of particles over time. Applications include tracking of chemical pollutants [3], fish larvae [4], [5], and algae [6], [7]. Commonly, a random-walk or random-flight model is used to simulate particle trajectories (see, for example [8], [9], [10], [11]); these approaches are reviewed in [12]. LPT has also been shown to effectively model the motions of macroscopic (1-2 meter) drifting platforms deployed in the ocean [13], [14], [15], [16]. However, the effectiveness of LPT is sensitive to the initial positions of the deployed platforms and to the structure of the underlying flow [17], [18], [19]. Significant errors in predicted particle positions are also produced by errors in the modeled flow velocities; these may be caused by numerical error within ocean models, missing physics, insufficient resolution of the model in the region of interest, and errors in the model forcing. When a larger ocean model is used to drive a regional model, as is commonly done, errors in the forcing result in complex, multi-scale errors in the driven model; this is known as the uncertainty cascade [20], [21]. Multiple ocean models may be combined in a *hyper-ensemble* to improve the modeling of the surface drift [21]. Data collected from free-drifting sensor platforms can be assimilated into ocean models, improving the long-term accuracy of predicted flow values in certain cases [2], [17], [22], [18].

In recent years, autonomous underwater vehicles (AUVs) have been developed as small, inexpensive, and flexible controlled platforms that can support various oceanographic studies. AUVs have many of the same advantages as Lagrangian floats, hence can be used to replace Lagrangian floats in certain applications [23], [24]. Furthermore, AUVs are able to make real-time adjustments to mission goals, for example to increase sampling density in a particular region of interest, or navigate to study a specific phenomenon that has arisen during the deployment. In addition, the quality of collected data can be improved by combining measurements from multiple AUVs ([25], [26]), and the number of vehicles used is readily scalable [23]. This has led to research in cooperative adaptive sampling ([26], [27]) that has demonstrated new opportunities for ocean science and control theory enabled by AUV technologies.

The use of ocean model data for AUV navigation has been demonstrated by a number of research efforts. Various algorithms have been proposed for navigation guided by ocean model flow data, including use of the A* algorithm for min-time path planning under spatially-varying, time-static flow [28], [29]; Fast Marching (FM)-based algorithms for efficient path planning in a static flow field [30] (this method is generalized by Soulignac *at al*, to strong [31] and time-varying flows [32]); genetic algorithms [33], [34], [35]; and case-based path planning [36].

In the Adaptive Sampling and Prediction (ASAP) experiment [27], a fleet of underwater gliders (which are buoyancy-propelled AUVs), was used for cooperative sampling of a domain over the course of six weeks. The glider trajectories were generated based on flow predictions from ocean models, and adapted to changing flow conditions [26], [27], [37], [38]. A series of algorithms for ocean-model based control of an AUV for plume tracking using the Regional Ocean Model System (ROMS) is demonstrated in [39]. Collected flow data were fed back into the model to improve accuracy of the flow forecasts. Alternative schemes for adaptive sampling with the goal of incorporating assimilation of data collected by vehicles into trajectory planning are proposed in [40], [41].

Autonomous underwater vehicles may prove to be an important asset in the continued development of ever more accurate ocean models. We envision possibilities of integrating the localization and navigation performance of underwater vehicles with ocean modeling, to improve both the navigation performance of the AUVs, and the accuracy of ocean model predictions. In this paper, we introduce the method of controlled Lagrangian particle tracking (CLPT). CLPT quantifies the offset between predicted and actual positions of Lagrangian particles under *active feedback control* moving in ocean flows with the guidance from ocean circulation models. In contrast with LPT, which deals with passively drifting particles, CLPT allows the particles to control their motion. CLPT creates a natural framework for understanding the interaction between flows estimated or predicted by ocean models and controlled particle trajectories. Incorporating feedback control helps to overcome some of the difficulties encountered in the method of LPT.

We consider the offset between the physical positions and the simulated positions as CLPT error. The main contribution of this paper is to reveal and theoretically justify the unique characteristics of the error growth associate with the CLPT that has not been previously observed in LPT. We show that the CLPT error typically grows exponentially for a relatively short period of time until it reaches a turning point. Afterwards, the CLPT error will grow much slower with

a rate bounded above by polynomial functions of time. The size of error at the turning point is given by a function that only depends on the resolution of the ocean model. These behaviors of the CLPT error are theoretically justified under simplifying assumptions about the dynamics of the CLPT particles and structure of the error in the ocean model. As comparison, the error growth for LPT tend to be exponential most of the time. The difference between the error growth rate can also be explained theoretically. Our results show that CLPT error grows much slower than LPT error, and hence may be more useful for ocean model improvements and vehicle navigations in certain situations. In addition, we show that although our theoretical results are derived under simplifying assumptions, they are consistent with data collected from controlled underwater gliders during the adaptive sampling and prediction (ASAP) field experiment performed in Monterey Bay, CA, in 2006.

The rest of this paper is organized as follows. The method of the controlled Lagrangian particle tracking and CLPT error is introduced in Section II. The upper threshold for exponential growth of the CLPT error is calculated in Section III for the 1-D and 2-D flow cases. Long-term particle tracking error due to small-scale turbulent flows not resolved by the ocean model is considered in Section IV. The results are compared with simulation and observations made during the Adaptive Sampling and Prediction (ASAP) experiment in Monterey Bay in 2006 (Section V). This paper significantly extends our preliminary results for the 1-D case presented in [42], [43].

II. Controlled Lagrangian Particle Tracking

Controlled Lagrangian particle tracking is used to model the motions of vehicles with controlled velocity inputs in ocean flow fields. Each vehicle is modeled as a massless particle whose velocity is the sum of ambient flow velocity $\mathcal{F}$ and control velocity input $\mathbf{u}$. In this paper, we consider the horizontal motion of the particles. Particle position at time t is given by $\mathbf{x}(t) \in \mathcal{D} \subset \mathbb{R}^2$, obtained by integrating the following equation:

$$\mathrm{d}\mathbf{x}(t) = (\mathcal{F}(\mathbf{x}, t) + \mathbf{u}(\mathbf{x}, t))\,\mathrm{d}t \tag{1}$$

Realistic trajectories for particles drifting in a flow field can be simulated by using a statistical approach to particle tracking, where the flow field $\mathcal{F}$ is decomposed into two constituent components: a mean flow $\mathbf{F}$, and a stochastic eddy diffusion field ν, that includes small-scale flow fluctuations due to physical eddies, as well as waves, wind-driven flows, and other turbulent

components. It has been shown that this approach can be used effectively to model trajectories of passive drifter platforms in the ocean, provided that the parameters describing the turbulent flow components are known or can be estimated [12], [44], [45]. A good first-order model of particle trajectories can be given by a Markovian random-flight model, described using the Langevin equation from [44], with added control velocity term $\mathbf{u}$:

$$\begin{aligned} \mathrm{d}\mathbf{x} &= (\mathbf{F}(\mathbf{x},t) + \nu + \mathbf{u}(\mathbf{x},t))\mathrm{d}t \\ \mathrm{d}\nu &= -A\nu\mathrm{d}t + \Lambda\mathrm{d}\omega \end{aligned} \tag{2}$$

where $\mathbf{F}(\mathbf{x},t)$ is the underlying mean flow, and ν is the eddy diffusion term. The matrices A and Λ are given by

$$A = \begin{bmatrix} \frac{1}{\tau} & \Omega \\ -\Omega & \frac{1}{\tau} \end{bmatrix} \qquad \Lambda = \begin{bmatrix} \sigma\sqrt{\frac{2}{\tau}} & 0 \\ 0 & \sigma\sqrt{\frac{2}{\tau}} \end{bmatrix} \tag{3}$$

where σ is the variance of the stochastic velocity fluctuations, τ represents Lagrangian correlation time, and Ω is the spin parameter. The stochastic input ω represents zero-mean, Gaussian white noise.

A natural approach to predicting the position of a controlled particle would be to obtain an estimate $\hat{\mathbf{F}}$ of the ocean flow field $\mathcal{F}$, using an ocean model. The estimated position $\mathbf{z}(t)$ of the particle is then governed by

$$\mathrm{d}\mathbf{z}(t) = \left(\hat{\mathbf{F}}(\mathbf{z},t) + \mathbf{u}(\mathbf{z},t)\right)\mathrm{d}t. \tag{4}$$

This equation can be integrated numerically for $\mathbf{z}(t)$.

A. CLPT Error

The more realistic model of particle motion in (2) can be used to gauge the accuracy of position prediction made using the simple model (4). The position prediction error $\mathbf{e}_{pos} \in \mathbb{R}^2$ is defined as difference between the predicted particle position $\mathbf{z}(t)$ and the position obtained using the Langevin model $\mathbf{x}(t)$:

$$\mathbf{e}_{pos}(t) = \mathbf{x}(t) - \mathbf{z}(t). \tag{5}$$

The initial conditions are set with initial time $t_0 = 0$, and $\mathbf{z}(0) = \mathbf{x}(0)$, so that $\mathbf{e}(0) = [0\ 0]^{\mathrm{T}}$. The magnitude of the position prediction error is defined as the CLPT error $e(t)$:

$$e(t) := \| \mathbf{x}(t) - \mathbf{z}(t) \|, \tag{6}$$

where $\|\cdot\|$ represents the standard ℓ^2 norm in $\mathbb{R}^2$, and $\mathbf{e}(0) = 0$. The CLPT error may be taken as a measure of the performance of the ocean-model based position prediction.

B. CLPT error dynamics

In the following section, we will show that there is a fundamental limit on the quality of the position prediction estimate that can be obtained using the ocean model for a particle moving under flow-canceling control. We show that the growth of error in predicted position is initially exponential; we derive an expected threshold for decrease in the error growth rate to polynomial growth.

The growth in the position estimation error over time is given by

$$\begin{aligned} \mathrm{d}\mathbf{e}_{pos}(t) &= [\mathbf{F}(\mathbf{x},t) + \mathbf{u}(\mathbf{x},t) - \hat{\mathbf{F}}(\mathbf{z},t) - \mathbf{u}(\mathbf{z},t) + \nu]\mathrm{d}t \\ \mathrm{d}\nu &= -A\nu\mathrm{d}t + \Lambda\mathrm{d}\omega. \end{aligned} \tag{7}$$

Let $\mathbf{f}(\mathbf{z},t) := \mathbf{F}(\mathbf{z},t) - \hat{\mathbf{F}}(\mathbf{z},t)$ be the error in the estimated mean flow $\hat{\mathbf{F}}$. The above equation may be written as

$$\mathrm{d}\mathbf{e}_{pos}(t) = [(\hat{\mathbf{F}}(\mathbf{x},t) + \mathbf{f}(\mathbf{x},t)) + \mathbf{u}(\mathbf{x},t) - \hat{\mathbf{F}}(\mathbf{z},t) - \mathbf{u}(\mathbf{z},t)]\mathrm{d}t + \nu\mathrm{d}t. \tag{8}$$

The control velocity $\mathbf{u}$ can be designed to cancel the effects of the mean flow; since the mean flow is not known, $\mathbf{u}$ can be set to cancel only the estimated mean flow. In the remainder of this paper, we will make the following assumption:

(A1) A flow-canceling controller has been implemented, so that:

$$\mathbf{u}(\chi,t) = -\hat{\mathbf{F}}(\chi,t) \tag{9}$$

for $\chi(t) = \mathbf{x}(t)$ or $\mathbf{z}(t)$.

Under assumption (A1),

$$[(\hat{\mathbf{F}}(\mathbf{x},t) + \mathbf{f}(\mathbf{x},t)) + \mathbf{u}(\mathbf{x},t) - \hat{\mathbf{F}}(\mathbf{z},t) - \mathbf{u}(\mathbf{z},t)] = \mathbf{f}(\mathbf{x},t) \tag{10}$$

for all times t. Position estimation error growth may therefore be modeled as

$$\begin{aligned} \mathrm{d}\mathbf{e}_{pos}(t) &= [\mathbf{f}(\mathbf{x},t) + \nu]\mathrm{d}t \\ \mathrm{d}\nu &= -A\nu\mathrm{d}t + \Lambda\mathrm{d}\omega, \end{aligned} \tag{11}$$

with initial condition $\mathbf{e}_{pos}(0) = [0\,0]^{\mathrm{T}}$.

In this section, we consider the error growth due to error in predicted flow $\mathbf{f}$ alone; we therefore make the assumption:

(A2) The small-scale eddy diffusivity is negligible, so that $\nu(t) \equiv 0$.

Under assumption (A2), the position estimation error evolves in times as

$$\frac{\mathrm{d}\mathbf{e}_{pos}}{\mathrm{d}t} = \mathbf{f}(\mathbf{x}, t) \tag{12}$$

with $\mathbf{e}(0) = [0\ 0]^{\mathrm{T}}$. As $t \to \infty$, $\mathbf{e}_{pos}$ will converge to a stable equilibrium point of $\mathbf{f}(\mathbf{x}, t) = \mathbf{f}(\mathbf{z} + \mathbf{e}, t)$. In general $\mathbf{f}$ is an unknown function of position and time, whose values depend on the particular realization of the ocean flow and on the model used.

Given perfect cancellation of the model flow, the position of the virtual vehicle remains $\mathbf{z}(t) = \mathbf{z}(0)$. Therefore, $\mathbf{e}_{pos}(t) = \mathbf{x}(t) - \mathbf{z}(0)$. We can assume, without loss of generality, that the vehicle starts at the origin, $\mathbf{x}(0) = \mathbf{z}(0) = [0\ 0]^{\mathrm{T}}$. Then $\mathbf{e}_{pos}(t)$ given by (12) will be equal to $\mathbf{x}(t)$ in the following system:

$$\mathrm{d}\mathbf{x} = \mathbf{f}(\mathbf{x}, t)\mathrm{d}t, \qquad \mathbf{x}(0) = 0 \tag{13}$$

where $\mathbf{f}(\mathbf{x}, t) := \hat{\mathbf{F}}(\mathbf{x}, t) - \mathbf{F}(\mathbf{x}, t)$. For simplicity, we will ignore the time variation of $\mathbf{f}$ and treat it as a function of $\mathbf{x}$ only. We also assume that $\mathbf{f}$ has equilibria; that is, there exits a non-empty set $\mathbf{X}$ s.t. $f(\mathbf{x}, t) = 0\ \forall \mathbf{x} \in \mathbf{X}$.

For a given realization of $\mathbf{f}$, the motion of $\mathbf{x}(t)$ can be approximated using a linearization of (13),

$$\mathrm{d}\mathbf{x} \approx \mathbf{f}(0) + D_{\mathbf{x}}\mathbf{f}(0)\mathbf{x}\mathrm{d}t, \qquad \mathbf{x}(0) = 0 \tag{14}$$

where $D_{\mathbf{x}}\mathbf{f}$ is the Jacobian of $\mathbf{f}$. It is a well-known result that the trajectories of such a linear time-invariant system have the form

$$\mathbf{x}(t) = e^{D_{\mathbf{x}}\mathbf{f}(0)t} \int_0^t e^{-D_{\mathbf{x}}\mathbf{f}(0)\tau}\mathbf{f}(0)\mathrm{d}\tau, \tag{15}$$

which corresponds to exponential error growth. Suppose that $\mathbf{x}(t)$ in (13) approaches $\mathbf{x}_{eq}$, a stable equilibrium of (13), as $t \to \infty$. Then $\| \mathbf{x}_{eq} - \mathbf{z}(0) \| = \| \mathbf{x}_{eq} \|$ is an upper threshold for exponential growth of the CLPT error.

C. Comparison with LPT error

For freely-drifting agents in the ocean, the position prediction error can be expressed as in (7), with control $\mathbf{u} \equiv 0$:

$$\begin{aligned} \mathrm{d}\mathbf{e}_{pos}(t) &= [\mathbf{F}(\mathbf{x},t) - \mathbf{F}(\mathbf{z},t)]\mathrm{d}t - \mathbf{f}(\mathbf{z},t)\mathrm{d}t + \nu \mathrm{d}t \\ \mathrm{d}\nu &= -A\nu \mathrm{d}t + \Lambda \mathrm{d}\omega. \end{aligned} \tag{16}$$

The first term in the error growth equation depends on the underlying flow velocity at two different points: the simulated vehicle position $\mathbf{z}(t)$ and the true position $\mathbf{x}(t)$. Given a slight initial offset between $\mathbf{z}$ and $\mathbf{x}$, the error growth due to this term alone (setting $\mathbf{f} \equiv 0$ and $\nu \equiv 0$) is:

$$\mathrm{d}\mathbf{e}_{pos}(t) = [\mathbf{F}(\mathbf{x},t) - \mathbf{F}(\mathbf{z},t)]\mathrm{d}t. \tag{17}$$

This can be interpreted as the offset between two particles, initially close together, drifting in an ocean flow. It is a well-known result in oceanography that, even in simple flow fields, the separation between two such particles may grow exponentially without bound (this fast divergence of trajectories from close initial conditions is termed deterministic chaos) [2]. Thus, nothing can be said about the long-term error growth rate. This is in contrast with the case of controlled particles, where error growth rate will be shown to decrease in the long term.

III. Theoretical threshold on exponential growth of CLPT Error

In this section, we derive the expected upper thresholds for exponential growth of CLPT error, for one and two-dimensional flow fields. The expected thresholds are functions of the gridsize in the ocean model used to estimate the flow.

A. The one dimensional case

We first consider the case when flow is one-dimensional, and compute a theoretic upper threshold on exponential growth of the CLPT error; this threshold is given by $E(|\mathbf{x}_{eq} - \mathbf{z}(0)|)$, since $\mathbf{x}$ asymptotically converges to $\mathbf{x}_{eq}$. We make the following assumptions:

(B1) The particle is confined to move on a line, so the domain of $\mathbf{f}$ is $\mathbb{R}$. Since $\mathbf{f}$ is now a scalar function, we denote it by f; similarly, we denote the real and virtual particle positions $\mathbf{x}$ and $\mathbf{z}$ by x and z, respectively.

(B2) We define a grid over $\mathbb{R}$, with uniform gridsize h. The ocean model outputs an estimate $\hat{F}$ of the flow F at each gridpoint $x_k = kh$. We model the values of $f(x) = \hat{F}(x) - F(x)$ at the grid points are independent identically distributed noises[1]. The noise values are denoted as ξ_k ($\xi_k = f(x_k) = f(kh)$). These ξ_k are assumed to be symmetrically distributed around 0, with probability density function ρ_ξ.

(B3) The initial conditions are given by $x(0) = z(0) = 0$.

The values of f are not known everywhere in $\mathbb{R}$, since they depend on the structure of the unknown flow $\mathbf{F}$, as well as on the method used to interpolate $\hat{\mathbf{F}}$ between gridpoints. However, f can be approximated at any point by taking the linear interpolation of its values at the gridpoints: for $x \in (x_k, x_{k+1})$, we have

$$f(x) = \frac{(x_{k+1} - x)\,\xi_k + (x - x_k)\,\xi_{k+1}}{h}. \tag{18}$$

Under assumptions (B1)-(B3), the equilibria of $f(x)$ are given by

$$x_{eq} = (\xi_{k+1}x_k - \xi_k x_{k+1})/(\xi_{k+1} - \xi_k). \tag{19}$$

We will find the expected threshold for exponential growth of CLPT error, $E(|x_{eq}|)$, over all realizations of the model flow f. For this, we need the following lemmas:

Lemma III.1. *The position x_{eq} in (19) is a stable equilibrium of (13) under assumptions (B1)-(B3) if and only if $\xi_k > 0$ and $\xi_{k+1} < 0$.*

Proof: A sufficient and necessary condition for x_{eq} to be a stable equilibrium is that it satisfies $f(x_{eq}) = 0$ and $\partial f/\partial x(x_{eq}) = (\xi_{k+1} - \xi_k)/h < 0$.

Suppose that $\xi_k > 0$ and $\xi_{k+1} < 0$. Clearly, there exists a point $x_{eq} \in [hk, h(k+1)]$, given by (19), which is an equilibrium of f. Since $(\xi_{k+1} - \xi_k)/h < 0$, x_{eq} must be a stable equilibrium.

Conversely, suppose that $x_k < x_{eq} < x_{k+1}$ is a stable equilibrium. Using the equation for x_{eq}, and the fact that $(\xi_{k+1} - \xi_k)/h < 0$, we get:

$$x_k < \quad \tfrac{\xi_{k+1}x_k - \xi_k x_{k+1}}{\xi_{k+1} - \xi_k} \quad < x_{k+1} \tag{20}$$

$$x_k(\xi_{k+1} - \xi_k) > \quad \xi_{k+1}x_k - \xi_k x_{k+1} \quad > x_{k+1}(\xi_{k+1} - \xi_k). \tag{21}$$

[1]Note that, for any given realization of the ocean model and true ocean flow fields, the flow error f is a deterministic, unknown function. By a small abuse of notation, we use f to denote the random variable whose value is a function over $\mathbb{R}^1$

Subtracting the middle term from both sides of (21), we find:

$$\xi_k(x_{k+1} - x_k) > 0 > \xi_{k+1}(x_{k+1} - x_k), \tag{22}$$

which directly gives $\xi_k > 0$, $\xi_{k+1} < 0$, since $x_{k+1} - x_k = h > 0$. This proves the Lemma.

■

Lemma III.2. *The probability that $x_{eq} \in (x_k, x_{k+1})$ given $\xi_0 > 0$ is:*

$$\mathbf{Pr}(x_{eq} \in (x_k, x_{k+1}) | \xi_0 > 0) = \left(\frac{1}{2}\right)^{k+1}.$$

Proof: By Claim III.1, $\mathbf{Pr}(x_{eq} \in (x_k, x_{k+1}) | \xi_0 > 0)$ is simply the probability that $\xi_1, ..., \xi_k > 0$ and $\xi_{k+1} < 0$. Because the values of ξ are independent,

$$\mathbf{Pr}(\xi_1, ..., \xi_k > 0, \xi_{k+1} < 0) = \left(\prod_i^k \mathbf{Pr}(\xi_i > 0)\right) \mathbf{Pr}(\xi_{k+1} < 0).$$

The ξ_i are iid symmetrically-distributed variables, thus $\mathbf{Pr}(\xi_i > 0) = 1/2$ for all i. Similarly, $\mathbf{Pr}(\xi_{k+1} < 0) = 1/2$. Thus $\mathbf{Pr}(x_{eq} \in (x_k, x_{k+1}) | \xi_0 > 0) = (1/2)^{k+1}$. ■

We now calculate $E(|x_{eq}|)$, where x_{eq} is a stable equilibrium of (18) such that $x \to x_{eq}$ as $t \to \infty$. By definition,

$$E(|x_{eq}|) = \int_0^\infty |x| \rho_{|x_{eq}|}(x) \mathrm{d}x \tag{23}$$

where $\rho_{|x_{eq}|}(x)$ is the probability density function of $|x_{eq}|$. We introduce ξ_0 as a conditioning variable in (23); then, using the fact that ξ_k are symmetrically-distributed, zero-mean random variables, so that

$$\mathbf{Pr}(\xi_k > 0) = \mathbf{Pr}(\xi_k < 0) = \int_0^\infty \rho_\xi(x) \mathrm{d}x = 1/2, \tag{24}$$

we have

$$E(|x_{eq}|) = \frac{1}{2} \int_0^\infty |x| \rho_{|x_{eq}|}(x | \xi_0 > 0) \mathrm{d}x + \frac{1}{2} \int_0^\infty |x| \rho_{|x_{eq}|}(x | \xi_0 < 0) \mathrm{d}x. \tag{25}$$

For convenience, we define the following variables:

$$x_+ = \mathrm{argmin}_{x>0}\{|x| : f(x) = 0, \partial f/\partial x < 0\} \tag{26}$$

$$x_- = \mathrm{argmin}_{x<0}\{|x| : f(x) = 0, \partial f/\partial x < 0\}. \tag{27}$$

The calculation of $E(|x_{eq}|)$ proceeds through the following three claims:

Claim III.1. *If $\xi_0 > 0$, then $x_{eq} = x_+$, and moreover, $x_{eq} \in (x_k, x_{k+1})$ where x_{k+1} is the position corresponding to the first negative value of ξ; that is, $\xi_j > 0$ for all $j \in \{1, 2, ..., k\}$, and $\xi_{k+1} < 0$.*

Proof: By the definition in (18), f is a continuous, piecewise affine function.

By continuity, $f(0) = \xi_0 > 0$ implies that $f > 0$ in some sufficiently small neighbourhood ϵ of 0. Thus x cannot become negative, since $dx/dt = f(x) > 0$ for all $x \in \epsilon$; so $\lim_{t\to\infty} x(t) = x_{eq} > 0$.

Since f is piecewise affine, $f > 0$ on any interval $[x_k, x_{k+1}]$ with ξ_k, $\xi_{k+1} > 0$, and f must have a zero-crossing x_{eq} on any interval (x_k, x_{k+1}) with $\xi_k > 0$ and $\xi_{k+1} < 0$. By Lemma III.1, this crossing is a stable equilibrium of (13). The smallest such crossing is x_+. Since $x = 0$ is in the region of attraction, $x \to x_{eq}$ as $t \to \infty$, thus $x_{eq} = x_+$. ■

Claim III.2. *If $\xi_0 < 0$, then $x_{eq} = x_-$, and moreover, $x_{eq} \in (x_{-k}, x_{-k+1})$ where x_{-k} is the point corresponding to the first positive value of ξ, that is, $\xi_j < 0$ for all $j \in \{-1, -2, ..., -k + 1\}$, and $\xi_{-k} > 0$.*

Proof: The proof exactly parallels the proof of Claim III.1. ■

Claim III.3. *Under assumptions (B1)-(B3) of the one-dimensional problem, we have*

$$\int_0^\infty |x|\rho_{|x_{eq}|}(x|\xi_0 > 0)\mathrm{d}x = \int_{-\infty}^0 |x|\rho_{|x_{eq}|}(x|\xi_0 < 0)\mathrm{d}x = \frac{3}{2}h.$$

Therefore, by (25), $E(|x_{eq}|) = \frac{3}{2}h$.

Proof: The statement $\int_0^\infty |x|\rho_{|x_{eq}|}(x|\xi_0 > 0)\mathrm{d}x = \int_{-\infty}^0 |x|\rho_{|x_{eq}|}(x|\xi_0 < 0)\mathrm{d}x$ follows from the symmetry of ρ_ξ. It remains to show that $E(|x_{eq}|) = 3h/2$.

Equation (25) for the expected value of $|x_{eq}|$ may be written as

$$E(|x_{eq}|) = \int_0^\infty |x|\rho_{|x_{eq}|}(x|\xi_0 > 0)\mathrm{d}x,$$

which can be decomposed as

$$E(|x_{eq}|) = \sum_{k=0}^{\infty} \int_{x_k}^{x_{k+1}} x\rho_{|x_{eq}|}(x|\xi_0 > 0, x_{eq} \in (x_k, x_{k+1}))\mathrm{d}x\mathbf{Pr}(x_{eq} \in (x_k, x_{k+1})|\xi_0 > 0). \quad (28)$$

Using Lemma III.2, and applying a change of variables $u = x - x_k$, we can write (28) as

$$E(|x_{eq}|) = \sum_{k=0}^{\infty} \left[\frac{1}{2}\right]^{k+1} \int_0^h (u + x_k)\rho_{|x_{eq}-x_k|}(u|\xi_0 > 0, (x_{eq} - x_k) \in (0, h))\mathrm{d}u. \quad (29)$$

We now compute $\rho_{|x_{eq}-x_k|}(u|\xi_0 > 0, (x_{eq} - x_k) \in (0,h))$. Given that $x_{eq} \in (x_k, x_{k+1})$, let $u_* \triangleq x_{eq} - x_k$ in this interval. To find $\rho_{u_*}(u|u_* \in (0,h))$, the probability density of u_* in terms of u, we consider the mapping $\phi : \mathbb{R}^2 \to \mathbb{R}^2 : (\xi_k, \xi_{k+1}) \mapsto (u_*, v)$, where

$$u_* = \frac{h\xi_k}{\xi_k - \xi_{k+1}} \tag{30}$$

$$v = \xi_k. \tag{31}$$

Let $\vec{\xi}$ denote the doublet (ξ_k, ξ_{k+1}), and $\vec{w}$ denote (u_*, v). The distribution of $\vec{w}$ is given by

$$\tilde{\rho}(\vec{w}) = \left|\det \frac{\partial \phi}{\partial \vec{\xi}}\right|^{-1} \rho(\phi^{-1}(\vec{w})). \tag{32}$$

The inverse map is well-defined and is given by

$$\phi^{-1}(\vec{w}) = (\xi_k, \xi_{k+1}) = (v, v(1 - h/u_*)), \tag{33}$$

while

$$\left|\det \frac{\partial \phi}{\partial \vec{\xi}}\right|^{-1} = \left|\det \begin{pmatrix} -\frac{h\xi_{k+1}}{(\xi_k - \xi_{k+1})^2} & \frac{h\xi_k}{(\xi_k - \xi_{k+1})^2} \\ 1 & 0 \end{pmatrix}\right|^{-1} = \frac{(\xi_k - \xi_{k+1})^2}{h\xi_k} = \frac{hv}{u_*^2}. \tag{34}$$

Substituting (34) and (33) into (32), we have:

$$\tilde{\rho}(\vec{w}) = \frac{hv}{u_*^2}\rho(v, v(1 - h/u_*)). \tag{35}$$

Since ξ_k and ξ_{k+1} are independent, symmetrically distributed random variables and $\xi_k > 0$ and $\xi_{k+1} < 0$ are given, we have:

$$\rho(\xi_k) = 2\rho_\xi(\xi_k)U(\xi_k) \tag{36}$$

$$\rho(\xi_{k+1}) = 2\rho_\xi(\xi_{k+1})U(-\xi_{k+1}), \tag{37}$$

where $U(\cdot)$ denotes the unit step function.

Because the values of ξ are iid, the joint probability distribution

$$\rho(\phi^{-1}(\vec{\omega})) = \rho(\vec{\xi}) = \rho(\xi_k)\rho(\xi_{k+1}) = \rho(v)\rho(v(1 - h/u_*)). \tag{38}$$

Thus, using (36)-(37), (35) may be written as

$$\tilde{\rho}(\vec{w}) = \frac{4hv}{u_*^2}\rho_\xi(v)\rho_\xi(v(1 - h/u_*))U(v)U(v(h/u_* - 1)). \tag{39}$$

Taking the marginal distribution over v gives the distribution function $\rho_{|x_{eq}-x_k|}(u|(x_{eq}-x_k)\in(0,h))$ in (29):

$$\rho_{|x_{eq}-x_k|}(u|(x_{eq}-x_k)\in(0,h)) = \int_{-\infty}^{\infty}\tilde{\rho}(\vec{w})\mathrm{d}v = \frac{4h}{u_*^2}\int_0^{\infty} v\rho_\xi(v)\rho_\xi(v(1-h/u_*))\mathrm{d}vU(h/u_*-1). \quad (40)$$

Plugging in the above result in (29), we get:

$$\begin{aligned} E(|x_{eq}|) &= \sum_{k=0}^{\infty}\left[\frac{1}{2}\right]^{k+1}\int_0^h \frac{4h(u+x_k)}{u^2}\left(\int_0^{\infty} v\rho_\xi(v)\rho_\xi(v(1-h/u))\mathrm{d}v\right)\mathrm{d}u \\ &= \sum_{k=0}^{\infty}\left[\frac{1}{2}\right]^{k+1}\left(\int_0^h \frac{4hu}{u^2}\left(\int_0^{\infty} v\rho_\xi(v)\rho_\xi(v(1-h/u))\mathrm{d}v\right)\mathrm{d}u\right. \quad (41) \\ &\quad \left. + \int_0^h \frac{4hx_k}{u^2}\left(\int_0^{\infty} v\rho_\xi(v)\rho_\xi(v(1-h/u))\mathrm{d}v\right)\mathrm{d}u\right) \end{aligned}$$

This expression contains two integrals which will be handled in turn. Consider first the integral

$$\int_0^h \frac{4hx_k}{u^2}\left(\int_0^{\infty} v\rho_\xi(v)\rho_\xi(v(1-h/u))\mathrm{d}v\right)\mathrm{d}u. \quad (42)$$

After pulling out constants and reversing the order of integration, this becomes:

$$4x_k\int_0^{\infty} v\left(\int_0^h \frac{h}{u^2}\rho_\xi(v(1-h/u))\mathrm{d}u\right)\rho_\xi(v)\mathrm{d}v \quad (43)$$

Using change of variables $s = v(1-h/u)$, the above expression may be written as

$$4x_k\int_0^{\infty} v\left(\int_{-\infty}^0 \frac{(v-s)^2}{hv^2}\rho_\xi(s)\frac{hv}{(v-s)^2}\mathrm{d}s\right)\rho_\xi(v)\mathrm{d}v = 4x_k\int_0^{\infty}\left(\int_{-\infty}^0 \rho_\xi(s)\mathrm{d}s\right)\rho_\xi(v)\mathrm{d}v. \quad (44)$$

Because ρ_ξ is symmetric, $\int_{-\infty}^0\rho_\xi(s)\mathrm{d}s = \int_0^{\infty}\rho_\xi(v)\mathrm{d}v = 1/2$, and the above integral evaluates to $2x_k\int_0^{\infty}\rho_\xi(v)\mathrm{d}v = 2x_k(1/2) = x_k$.

Similarly, we can evaluate the integral

$$\int_0^h \frac{4hu}{u^2}\left(\int_0^{\infty} v\rho_\xi(v)\rho_\xi(v(1-h/u))\mathrm{d}v\right)\mathrm{d}u. \quad (45)$$

We again reverse the order of integration and pull out constants to get:

$$4\int_0^{\infty}\left(\int_0^h \frac{hv}{u}\rho_\xi(v(1-h/u))\mathrm{d}u\right)\rho_\xi(v)\mathrm{d}v. \quad (46)$$

Once again letting $s = v(1-h/u)$, we get:

$$4\int_0^{\infty}\left(\int_{-\infty}^0 (v-s)\rho_\xi(s)\frac{hv}{(v-s)^2}\mathrm{d}s\right)\rho_\xi(v)\mathrm{d}v = 4\int_0^{\infty}\int_{-\infty}^0 \frac{hv}{v-s}\rho_\xi(s)\rho_\xi(v)\mathrm{d}s\mathrm{d}v. \quad (47)$$

It can be shown, using the symmetry of ρ_ξ, that the above equation evaluates to $\frac{h}{2}$.

Therefore,

$$\begin{aligned} E(|x_{eq}|) &= \sum_{k=0}^{\infty} \left[\frac{1}{2}\right]^{k+1} \int_0^h \frac{4h(u+x_k)}{u^2} \left(\int_0^\infty v\rho_\xi(v)\rho_\xi(v(1-h/u_*))\mathrm{d}v \right) \mathrm{d}u \\ &= \sum_{k=0}^{\infty} \left(\frac{1}{2}\right)^{k+1} \frac{h}{2} + \sum_{k=0}^{\infty} \left(\frac{1}{2}\right)^{k+1} x_k \\ &= \frac{h}{4} \sum_{k=0}^{\infty} \left(\frac{1}{2}\right)^{k} + \frac{h}{2} \sum_{k=0}^{\infty} \left(\frac{1}{2}\right)^{k} k \\ &= \frac{h}{2} + h = \frac{3}{2}h, \end{aligned} \tag{48}$$

where we have used $x_k = kh$. This proves Claim III.3. ■

We now extend the above result to the case where the particle's initial position does not coincide with a particular gridpoint (that is, we drop assumption (B3)). Suppose that the particle's initial position is $x(0) = z(0) \in (x_k, x_{k+1}]$. There are then 4 possible cases, depending on the values of $\xi_k = f(x_k)$ and $\xi_{k+1} = f(x_{k+1})$:

1) $\xi_k > 0$ and $\xi_{k+1} > 0$,
2) $\xi_k < 0$ and $\xi_{k+1} > 0$,
3) $\xi_k > 0$ and $\xi_{k+1} < 0$,
4) $\xi_k < 0$ and $\xi_{k+1} < 0$.

Let c be a random variable that labels the above cases; c takes values in the set $\{1, 2, 3, 4\}$, with $\mathbf{Pr}(c = i) = \frac{1}{4}$ for all i. The expected value of $|x_{eq} - x(0)|$ in this case may be calculated using conditional expectations:

$$E(|x_{eq} - x(0)|) = \frac{1}{4} \sum_{i=1}^{4} E(\,|x_{eq} - x(0)||\, c = i). \tag{49}$$

Claim III.4. *The expected value of $|x_{eq} - x(0)|$ is independent of initial conditions, that is,*

$$E(|x_{eq} - x(0)|) = 3h/2 \tag{50}$$

for arbitrary $x(0) = z(0)$.

Proof: We proceed by calculating $E(\,|x_{eq} - x(0)||\, c = i)$ for each case in turn.

To begin, consider case 1) ($\xi_k > 0$ and $\xi_{k+1} > 0$). By monotonicity of f on (x_k, x_{k+1}), $f(x) > 0$ for all $x \in (x_k, x_{k+1}]$; it is clear, then, that the particle moves in the positive x-direction until it passes x_{k+1}; the expected distance to the nearest equilibrium is then

$$E(x_{eq} - x(0)) = E(x_{eq} - x_{k+1}) + x_{k+1} - x(0) \tag{51}$$

where $x_{k+1} > 0$ is given. Shifting the origin to x_{k+1} and using Claim III.3 gives $E(x_{eq} - x_{k+1}) = 3h/2$. Plugging this back into (51) gives

$$E(\,|x_{eq} - x(0)|\,|\,c = 1) = 3h/2 + (x_{k+1} - x(0)). \tag{52}$$

Case 4) ($\xi_k < 0$ and $\xi_{k+1} < 0$) is analogous to case 1); this time however, $f(x) < 0$ for all $x \in (x_k, x_{k+1}]$. The particle moves in the negative x-direction until it passes x_k, therefore

$$E(\,|x_{eq} - x(0)|\,|\,c = 4) = (x(0) - x_k) + 3h/2. \tag{53}$$

Next consider case 2) ($\xi_k < 0$ and $\xi_{k+1} > 0$). Here we can calculate the expectation as follows:

$$\begin{aligned} E(\,|x_{eq} - x(0)|\,|\,c = 2) =& E(\,|x_{eq} - x(0)|\,|\,c = 2,\, f(x(0)) > 0)\mathbf{Pr}(f(x(0)) > 0) \\ &+ E(\,|x_{eq} - x(0)|\,|\,c = 2,\, f(x(0)) < 0)\mathbf{Pr}(f(x(0)) < 0). \end{aligned} \tag{54}$$

If $f(x(0)) = f(z(0)) > 0$, then $f(x) > 0$ for all $x \in (x(0), x_{k+1}]$; so the particle moves in the positive direction until it passes x_{k+1}. As in case 1), the expected value of $|x_{eq} - x(0)|$ is then $3h/2 + (x_{k+1} - x(0))$. If, on the other hand, $f(x(0)) = f(z(0)) < 0$, then $f(x) < 0$ for all $x \in (x_k, x(0))$, and the particle moves in the negative direction until it passes x_k. As in case 4), the expected value of $|x_{eq} - x(0)|$ is then $(x(0) - x_k) + 3h/2$. Therefore (54) can be rewritten as

$$\begin{aligned} E(\,|x_{eq} - x(0)|\,|\,c = 2) &= \left(\frac{3h}{2} + (x_{k+1} - x(0))\right)\mathbf{Pr}(f(x(0)) > 0) \\ &\quad + \left(\frac{3h}{2} + (x(0) - x_k)\right)(1 - \mathbf{Pr}(f(x(0)) > 0)) \\ &= \left(\frac{3h}{2} + x(0) - x_k\right) + (h - 2(x(0) - x_k))\mathbf{Pr}(f(x(0)) > 0). \end{aligned} \tag{55}$$

It remains only to calculate the probability $\mathbf{Pr}(f(x(0)) > 0)$. Let $y_0 := x(0) - x_k$ ($y_0 \in (0, h]$). Using (18), we can write:

$$\begin{aligned} \mathbf{Pr}(f(y_0) > 0 | \xi_k < 0, \xi_{k+1} > 0) &= \mathbf{Pr}\left(\frac{y_0\xi_{k+1} + (h - y_0)\xi_k}{h} > 0 \middle| \, \xi_k < 0, \xi_{k+1} > 0\right) \\ &= \mathbf{Pr}\left(\xi_{k+1} > \frac{y_0 - h}{y_0}\xi_k \middle| \, \xi_k < 0, \xi_{k+1} > 0\right). \end{aligned} \tag{56}$$

This can be calculated, using the fact that $\xi_k < 0$ and $\xi_{k+1} > 0$, as

$$\mathbf{Pr}\left(\xi_{k+1} > \frac{y_0 - h}{y_0}\xi_k \middle| \xi_k < 0, \xi_{k+1} > 0\right) = \int_{-\infty}^{0} \left(\int_{\frac{y_0-h}{y_0}s}^{\infty} \rho_\xi(r)dr\right) \rho_\xi(s)\mathrm{d}s. \tag{57}$$

Lastly, consider case 3) ($\xi_k > 0$ and $\xi_{k+1} < 0$). By Lemma 1, there is a stable equilibrium $x_{eq} \in (x_k, x_{k+1})$ where $f(x_{eq}) = 0$. By monotonicity of f within one interval, we have that if $f(x(0)) < 0$, then $x(0) > x_{eq}$; and if $f(x(0)) > 0$, then $x_{eq} > x(0)$. Therefore,

$$\begin{aligned}
&E(|x_{eq} - x(0)||c = 3) \\
&= E(x_{eq} - x(0))\mathbf{Pr}(f(x(0)) > 0) + E(x(0) - x_{eq})\mathbf{Pr}(f(x(0)) < 0) \\
&= (x_k + h/2 - x(0))\mathbf{Pr}(f(x(0)) > 0) \\
&\quad + (x(0) - (x_k + h/2))(1 - \mathbf{Pr}(f(x(0)) > 0)) \\
&= 2((x_k + h/2) - x(0))\mathbf{Pr}(f(x(0)) > 0) - ((x_k + h/2) - x(0))
\end{aligned} \tag{58}$$

where $\mathbf{Pr}(f(x(0)) > 0)$ denotes

$$\mathbf{Pr}(f(x(0)) > 0 | \xi_k > 0, \xi_{k+1} < 0),$$

that can be calculated analogously to the probability in case 2) (using $y_0 := x(0) - x_k$):

$$\mathbf{Pr}(f(y_0) > 0 | \xi_k > 0, \xi_{k+1} < 0) = 1 - \int_{0}^{\infty} \left(\int_{-\infty}^{\frac{y_0-h}{y-0}s} \rho_\xi(r)\mathrm{d}r\right) \rho_\xi(s)\mathrm{d}s \tag{59}$$

Using the fact that ρ_ξ is a symmetric function and applying change of variables $r' = -r$ and $s' = -s$, the above may be rewritten as

$$\begin{aligned}
\mathbf{Pr}(f(y_0) > 0 | \xi_k > 0, \xi_{k+1} < 0) &= 1 - \int_{-\infty}^{0} \left(\int_{\frac{y_0-h}{y-0}s}^{\infty} \rho_\xi(r)\mathrm{d}r\right) \rho_\xi(s)\mathrm{d}s \\
&= 1 - \mathbf{Pr}(f(y_0) > 0 | \xi_k < 0, \xi_{k+1} > 0).
\end{aligned} \tag{60}$$

Plugging (52),(53),(55), and (58) into (49) gives

$$E(|x_{eq} - x(0)|) = 3h/2, \tag{61}$$

which is independent of the value of $x(0)$. This proves Claim III.4. ■

B. The two dimensional case

We have shown that, in the one-dimensional case, $E(|x_{eq} - z(0)|) = 3h/2$. This result can be generalized to the two-dimensional case. The assumptions for this case are as follows:

(C1) The particle moves in the horizontal plane (the domain of $\mathbf{f}$ is $\mathbb{R}^2$).

(C2) The ocean model outputs an estimate $\hat{\mathbf{F}}$ of the flow $\mathbf{F}$ at each gridpoint on a uniform square grid over $\mathbb{R}^2$ with gridsize h, where $\mathbf{x}_{k,l} = [kh,\, lh]^{\mathrm{T}}$ is a gridpoint indexed by (k, l). We assume that the values of $\mathbf{f}(\mathbf{x}) = \hat{\mathbf{F}}(\mathbf{x}) - \mathbf{F}(\mathbf{x})$ at the grid points are iid symmetrically-distributed random variables, which will be denoted by $\vec{\xi}_{k,l} = [\xi^1_{k,l}\ \xi^2_{k,l}]^{\mathrm{T}}$ (where $\xi^1_{k,l} = f^1(\mathbf{x}_{k,l})$ and $\xi^2_{k,l} = f^2(\mathbf{x}_{k,l})$ are mutually independent). The pdf of $\xi^i_{k,l}$, where $i = 1, 2$, will be denoted by ρ_ξ.

(C3) The initial position of the particle in simulation is equal to the initial position of the physical particle: $\mathbf{z}(0) = \mathbf{x}(0)$.

Analogous to the one-dimensional case, values of $\mathbf{f}$ at any point can be approximated by taking the bilinear interpolation of grid point values; for $\mathbf{x} = [x^1\, x^2]^{\mathrm{T}} \in (kh, (k+1)h) \times (lh, (l+1)h)$, $\mathbf{f}$ is given by

$$\begin{aligned}\mathbf{f}(\mathbf{x}) = \frac{1}{h^2}\Bigg\{\Big[&\vec{\xi}_{k,l}((k+1)h - x^1)((l+1)h - x^2) + \vec{\xi}_{k+1,l}(x^1 - kh)((l+1)h - x^2) \\ &+ \vec{\xi}_{k,l+1}((k+1)h - x^1)(x^2 - lh) + \vec{\xi}_{k+1,l+1}(x^1 - kh)(x^2 - lh)\Big]\Bigg\}.\end{aligned} \tag{62}$$

In two dimensions, the particle exhibits a much richer range of behaviors than a particle confined to move on a line, and it becomes much more difficult to find $\lim_{t\to\infty} \mathbf{x}(t) = \mathbf{x}_{eq}$. Instead, we approximate this value by finding a lower bound on $E_f(|\mathbf{x}_{eq} - \mathbf{x}(0)|)$ as $E_f(|\mathbf{x}_* - \mathbf{x}(0)|)$, where $\mathbf{x}_*$ is defined as the smallest (w.r.t. the 1-norm in $\mathbb{R}^2$) equilibrium of the flow $\mathbf{f}$ that satisfies the necessary stability condition $\partial \mathbf{f}^i / \partial \mathbf{x}^i < 0$ for $i = 1, 2$:

$$\mathbf{x}_* = \mathrm{argmin}_{\mathbf{x}\in\mathbb{R}^2} \left\{ \| \mathbf{x} - \mathbf{x}(0) \|_1 : \partial \mathbf{f}^{\mathrm{i}} / \partial \mathbf{x}^{\mathrm{i}}(\mathbf{x}) < 0 \ \ \forall \mathrm{i} \right\} \tag{63}$$

The main contribution of this section is summarized in the following theorem:

Theorem III.1. *The expected value of the 1-norm of the steady-state position prediction error*

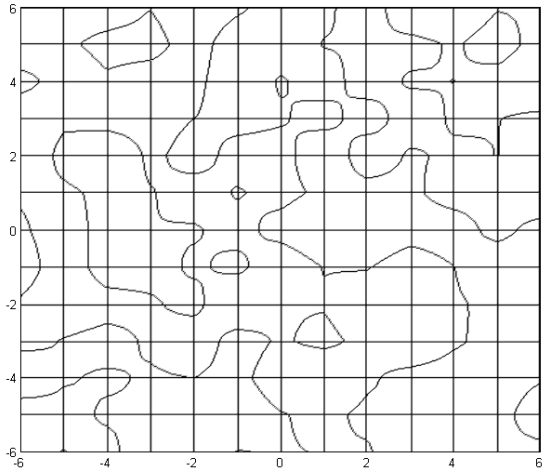

Fig. 1. Zero level set of the error flow in the x-direction, $\mathbf{f}^1(\mathbf{x}) = 0$. Equilibria of $\mathbf{f}(\mathbf{x})$ lie on intersections of the zero level sets for flow in the x- and y-directions.

given by $\| \mathbf{x}_* \|_1$ *satisfies:*

$$\begin{aligned} E(\| \mathbf{x}_* - \mathbf{x}(0) \|_1) \leq & 2 \sum_{k=0}^{\infty} \left\{ \frac{2(k+1)h}{4^{k+1}} \int_{-kh}^{-(k+1)h} \int_0^{\infty} \frac{4hv}{x^i} \rho_\xi(v) \rho_\xi(v(1-h/x^i)) \mathrm{d}v \mathrm{d}x^i \right. \\ & + \frac{2k}{4^{k+1}} \int_{-kh}^{-(k+1)h} \int_0^{\infty} \frac{4hv}{x^i} \rho_\xi(v) \rho_\xi(v(1-h/x^i)) \\ & \left. \times \left[1 - \int_0^{|x^i|-kh} \int_0^{\infty} \frac{4hv}{u^2} \rho_\xi(v) \rho_\xi(v(1-h/u)) \mathrm{d}v \mathrm{d}u \right] \mathrm{d}v \mathrm{d}x^i \right\} \end{aligned} \tag{64}$$

where h *is the grid size used by the ocean model. In particular, if* ρ_ξ *is Gaussian,*

$$E(\| \mathbf{x}_* - \mathbf{x}(0) \|_1) \leq 2.52h. \tag{65}$$

In order to prove this theorem, we need a sequence of lemmas, which are proved below. As in the one-dimensional case, we introduce the following variables for convenience:

$$x_+^i = \mathrm{argmin}_{x^i > 0} \{ |x^i| : f^i(x^i \hat{\mathbf{e}}_i) = 0, \partial f^i / \partial x^i < 0 \} \tag{66}$$

$$x_-^i = \mathrm{argmin}_{x^i < 0} \{ |x^i| : f^i(x^i \hat{\mathbf{e}}_i) = 0, \partial f^i / \partial x^i < 0 \}, \tag{67}$$

where $\hat{\mathbf{e}}_i$ is the i^{th} standard basis vector in $\mathbb{R}^2$.

Lemma III.3. *The value of* $\mathbf{Pr}(x_-^i \in (-(k+1)h, -kh) | \xi_{0,0}^i > 0)$ *is* $k \left(\frac{1}{2}\right)^{k+1}$.

Proof: The variable x^i_- represents the first stable equilibrium of f^i, evaluated on $(-\infty, 0)$ in the direction i. Without loss of generality, let $i = 1$ (x-axis). Along the axis, f^1 is a linear interpolation of its values at the points $\{0, \pm h, \pm 2h, \ldots\}$. By Claim III.1, the smallest stable equilibrium of f^1 on $(-\infty, 0)$ must lie in the first interval $((-(k+1)h, -kh))$ with $\xi^1_{-(k+1),0} > 0$ and $\xi^1_{-k,0} < 0$.

Since $\xi^1_{0,0} > 0$ by assumption, $\mathbf{Pr}(x^1_- \in (-h, 0)) = 0$. Let

$$\xi^1_{-j,0} = \min_{l \in \mathbb{Z}^+} \{\xi_{-l} : \xi_{-l} < 0\} \tag{68}$$

be the first negative gridpoint flow value. Then we have:

$$\mathbf{Pr}(x^1_- \in (-(k+1)h, -kh) | \xi^i_{0,0} > 0) = \\ \mathbf{Pr}(\xi^1_{-(k+1),0} > 0) \sum_{j=1}^{k} \Big(\prod_{m=j}^{k} \mathbf{Pr}(\xi^1_{-m,0} < 0) \prod_{l=1}^{j-1} \mathbf{Pr}(\xi^1_{-l,0} > 0) \Big) \tag{69}$$

By symmetry of the distribution of $\xi^1_{n,0}$, $\mathbf{Pr}(\xi^1_{n,0} > 0) = \mathbf{Pr}(\xi^1_{n,0} < 0) = 1/2$ for all n. The above equation may therefore be simplified to:

$$\mathbf{Pr}(x^1_- \in (-(k+1)h, -kh) | \xi^i_{0,0} > 0) = \sum_{i=1}^{k} \left(\frac{1}{2}\right)^{k+1} = k \left(\frac{1}{2}\right)^{k+1} \tag{70}$$

The calculation for x^2_- is analogous. This proves the Lemma. ■

Lemma III.4. *The value of* $\mathbf{Pr}(x^i_+ > (k+1)h | \xi^i_{0,0} > 0)$ *is* $\left(\frac{1}{2}\right)^{k+1}$.

Proof: The variable x^i_+ represents the first stable equilibrium of f^i, evaluated on the line corresponding to direction i. As in Lemma III.3, let $i = 1$ (x-axis). By Claim III.1, the smallest stable equilibrium of f^1 on $(0, \infty)$ must lie in the first interval $(mh, (m+1)h)$ with $\xi^1_{m,0} > 0$ and $\xi^1_{m+1,0} < 0$. Therefore, since $\xi^1_{0,0} > 0$ by assumption, $\mathbf{Pr}(x^1_+ > (k+1)h)$ is equal to the probability that $\xi^1_{i,0} > 0$ for all $i \in \{1, ..., k+1\}$. Using the fact that $\xi^1_{n,0}$ are independent and symmetrically distributed, we have:

$$\mathbf{Pr}(x^1_+ > (k+1)h | \xi^i_{0,0} > 0) = \prod_{i=1}^{k+1} \mathbf{Pr}(\xi^1_{i,0} > 0) = \left(\frac{1}{2}\right)^{k+1} \tag{71}$$

The calculation for x^2_+ is analogous. This proves the Lemma. ■

Lemma III.5. *The value of* $\mathbf{Pr}(x^i_+ \in (kh, (k+1)h) | \xi^i_{0,0} > 0)$ *is* $\left(\frac{1}{2}\right)^{k+1}$.

Proof: The proof is almost identical to that of Lemma III.4. Let $i = 1$ (x-axis). By Claim III.1, the smallest stable 0 of f^1 on $(0, \infty)$ must lie in the first interval $(kh, (k+1)h)$ with $\xi^1_{k,0} > 0$ and $\xi^1_{k+1,0} < 0$. Therefore, since $\xi^1_{0,0} > 0$ by assumption, $\mathbf{Pr}(x^1_+ > (k+1)h)$ is equal to the probability that $\xi^1_{i,0} > 0$ for all $i \in \{1, ..., k\}$, and $\xi^1_{k+1,0} < 0$. Using the fact that $\xi^1_{n,0}$ are independent and symmetrically distributed, we have:

$$\mathbf{Pr}(x^1_+ > (k+1)h | \xi^i_{0,0} > 0) = \prod_{i=1}^{k} \mathbf{Pr}(\xi^1_{i,0} > 0)\mathbf{Pr}(\xi^1_{k+1,0} < 0) = \left(\frac{1}{2}\right)^{k+1} \tag{72}$$

The calculation for x^2_+ is analogous. This proves the Lemma. ■

Lemma III.6. *The probability that x_* lies in the interval $(-(k+1)h, -kh)$ is:*

$$\mathbf{Pr}(x_* = x^i_-, x^i_- \in (-(k+1)h, -kh) | \xi^i_{0,0} > 0) = \frac{k}{4^{k+1}} + \frac{k}{4^{k+1}} \left(1 - \int_0^{|x^i_-|-kh} \frac{4h}{u^2} \left(\int_0^\infty v \rho_\xi(v) \rho_\xi(v(1-h/u)) \mathrm{d}v\right) \mathrm{d}u\right). \tag{73}$$

Proof: The value of $\mathbf{Pr}(x_* = x^i_-, x^i_- \in (-(k+1)h, -kh) | \xi^i_{0,0} > 0)$ is given by

$$\mathbf{Pr}(x_* = x^i_-, x^i_- \in (-(k+1)h, -kh) | \xi^i_{0,0} > 0) = \mathbf{Pr}(|x^i_-| < |x^i_+|, x^i_- \in (-(k+1)h, -kh) | \xi^i_{0,0} > 0). \tag{74}$$

The dependence on ξ_0 will not be written in future equations to avoid notational clutter, but will be assumed. The variables x^i_- and x^i_+ are mutually independent, so that

$$\begin{aligned} \mathbf{Pr}(|x^i_-| < |x^i_+|, x^i_- \in (-(k+1)h, -kh)) = & \\ \mathbf{Pr}(x^i_- \in (-(k+1)h, -kh))\mathbf{Pr}(x^i_+ > (k+1)h) & \\ + \mathbf{Pr}(x^i_- \in (-(k+1)h, -kh))\mathbf{Pr}(x^i_+ \in (|x^i_-|, (k+1)h)). & \end{aligned} \tag{75}$$

where

$$\mathbf{Pr}(x^i_+ \in (|x^i_-|, (k+1)h)) = \mathbf{Pr}(x^i_+ \in (|x^i_-|, (k+1)h) | x^i_+ \in (kh, (k+1)h))\mathbf{Pr}(x^i_+ \in (kh, (k+1)h)). \tag{76}$$

So that

$$\begin{aligned}&\mathbf{Pr}(|x_-^i| < |x_+^i|, x_-^i \in (-(k+1)h, -kh)) = \\ &\mathbf{Pr}(x_-^i \in (-(k+1)h, -kh))\mathbf{Pr}(x_+^i > (k+1)h) + \\ &\mathbf{Pr}(x_-^i \in (-(k+1)h, -kh))\mathbf{Pr}(x_+^i \in (|x_-^i|, (k+1)h)|x_+^i \in (kh, (k+1)h)) \\ &\quad \times \mathbf{Pr}(x_+^i \in (kh, (k+1)h)).\end{aligned} \tag{77}$$

Using Lemmas III.3-III.5, the above can be written as

$$\begin{aligned}&\mathbf{Pr}(|x_-^i| < |x_+^i|, x_-^i \in (-(k+1)h, -kh)) = \\ &\qquad \left(\frac{k}{4^{k+1}}\right) + \left(\frac{k}{4^{k+1}}\right)\mathbf{Pr}(x_+^i \in (|x_-^i|, (k+1)h)|x_+^i \in (kh, (k+1)h)).\end{aligned} \tag{78}$$

The remaining expression, $\mathbf{Pr}(x_+^i \in (|x_-^i|, (k+1)h)|x_+^i \in (kh, (k+1)h))$, may be calculated as follows:

$$\begin{aligned}&\mathbf{Pr}(x_+^i \in (|x_-^i|, (k+1)h)|x_+^i \in (kh, (k+1)h)) \\ &= 1 - \mathbf{Pr}(x_+^i \in (kh, |x_-^i|)|x_+^i \in (kh, (k+1)h)) \\ &= 1 - \int_{kh}^{|x_-^i|} \rho_{x_-^i}(x)\mathrm{d}x,\end{aligned} \tag{79}$$

where $x_-^i \in (kh, (k+1)h)$. Using the change of variables

$$\begin{aligned}u &= x - kh \\ v &= \xi_{k,0}^i\end{aligned} \tag{80}$$

and the distribution for $u_* = x_* - x_k = x_+ - kh$ derived in the one-dimensional case (see (40)), we have:

$$\begin{aligned}&\mathbf{Pr}(x_+^i \in (|x_-^i|, (k+1)h)|x_+^i \in (kh, (k+1)h)) \\ &= 1 - \int_0^{|x_-^i|-kh} \frac{4h}{u^2}\left(\int_0^\infty v\rho_\xi(v)\rho_\xi(v(1-h/u))\mathrm{d}v\right)\mathrm{d}u.\end{aligned} \tag{81}$$

Plugging this expression into (78), we can write:

$$\begin{aligned}&\mathbf{Pr}(x_* = x_-^i, x_-^i \in (-(k+1)h, -kh)) = \\ &\qquad \frac{k}{4^{k+1}} + \frac{k}{4^{k+1}}\left(1 - \int_0^{|x_-^i|-kh} \frac{4h}{u^2}\left(\int_0^\infty v\rho_\xi(v)\rho_\xi(v(1-h/u))\mathrm{d}v\right)\mathrm{d}u\right).\end{aligned} \tag{82}$$

This proves the Lemma. ■

Lemma III.7. *The probability that x_* lies in the interval $(kh,(k+1)h)$ is:*

$$\mathbf{Pr}(x_* = x_+^i, x_+^i \in (kh,(k+1)h)|\xi_{0,0}^i > 0) = \frac{k+2}{4^{k+1}} + \frac{k}{4^{k+1}}\left(1 - \int_0^{x_+^i - kh} \frac{4h}{u^2}\left(\int_0^\infty v\rho_\xi(v)\rho_\xi(v(1-h/u))\mathrm{d}v\right)\mathrm{d}u\right) \quad (83)$$

Proof: The value of $\mathbf{Pr}(x_* = x_+^i, x_+^i \in (kh,(k+1)h)|\xi_{0,0}^i > 0)$ is given by

$$\mathbf{Pr}(x_* = x_+^i, x_+^i \in (kh,(k+1)h)|\xi_{0,0}^i > 0) = \mathbf{Pr}(|x_+^i| < |x_-^i|, x_+^i \in (kh,(k+1)h)|\xi_{0,0}^i > 0). \quad (84)$$

For notational convenience, we refrain from writing the conditioning variable $\xi_{0,0}^i$. Using independence of x_-^i and x_+^i, the above equations may be written as

$$\begin{aligned}
&\mathbf{Pr}(|x_+^i| < |x_-^i|, x_+^i \in (kh,(k+1)h)) = \\
&\mathbf{Pr}(x_+^i \in (kh,(k+1)h))\mathbf{Pr}(x_-^i < -(k+1)h) + \\
&\mathbf{Pr}(x_+^i \in (kh,(k+1)h))\mathbf{Pr}(x_-^i \in (-(k+1)h, -x_+^i)|x_-^i \in (-(k+1)h,-kh)) \\
&\quad \times \mathbf{Pr}(x_-^i \in (-(k+1)h,-kh)).
\end{aligned} \quad (85)$$

By Lemmas III.3 and III.5,

$$\begin{aligned}
\mathbf{Pr}(x_+^i \in (kh,(k+1)h)) &= \left(\frac{1}{2}\right)^{k+1} \\
\mathbf{Pr}(x_-^i \in (-(k+1)h,-kh)) &= k\left(\frac{1}{2}\right)^{k+1},
\end{aligned} \quad (86)$$

and we can calculate

$$\begin{aligned}
\mathbf{Pr}(x_-^i < -(k+1)h) &= 1 - \sum_{j=0}^{k} \mathbf{Pr}(x_-^i \in (-(j+1)h,-jh)) \\
&= 1 - \sum_{j=0}^{k} j\left(\frac{1}{2}\right)^{j+1} \\
&= (k+2)\left(\frac{1}{2}\right)^{k+1}
\end{aligned} \quad (87)$$

Then using change of variables

$$\begin{aligned}
u &= x + (k+1)h \\
v &= \xi_{k,0}^i
\end{aligned} \quad (88)$$

and the distribution for $u_* = x_* - x_{-(k+1)} = x_+ + (k+1)h$ in (40), $\mathbf{Pr}(x^i_- \in (-(k+1)h, -x^i_+)|x^i_- \in (-(k+1)h, -kh))$ can be calculated analogously to $\mathbf{Pr}(x^i_+ \in (|x^i_-|, (k+1)h)|x^i_+ \in (kh, (k+1)h))$ to give:

$$\mathbf{Pr}(x^i_- \in (-(k+1)h, -x^i_+)|x^i_- \in (-(k+1)h, -kh)) = 1 - \int_0^{x^i_+ - kh} \frac{4h}{u^2} \left(\int_0^\infty v\rho_\xi(v)\rho_\xi(v(1-h/u))\mathrm{d}v \right) \mathrm{d}u \quad (89)$$

so that

$$\mathbf{Pr}(x_* = x^i_+, x^i_+ \in (kh, (k+1)h)) = \frac{k+2}{4^{k+1}} + \frac{k}{4^{k+1}} \left(1 - \int_0^{x^i_+ - kh} \frac{4h}{u^2} \left(\int_0^\infty v\rho_\xi(v)\rho_\xi(v(1-h/u))\mathrm{d}v \right) \mathrm{d}u \right). \quad (90)$$

This proves the Lemma. ■

Having these Lemmas, we can now proceed to the proof of Theorem III.1:

Proof: The ℓ^1 norm of $\mathbf{x}_*$ is $|x^1_*| + |x^2_*|$. By assumption, the flows along the x- and y-axes are mutually independent. We proceed by computing the expected value of $|x^i_*|$, for $i = 1, 2$, along each dimension independently.

First, note that the value of $E(|x_{*,i} - x_i(0)|)$ is independent of the initial position $\mathbf{x}(0)$. This can be shown as follows:

First, use a shift the coordinates; for $x_i(0) \in [kh, (k+1)h)$, let $x \mapsto x' = x - kh$ so that $x'_i(0) \in [0, h)$. Then

$$\begin{aligned} E(|x_{*,i} - x_i(0)|) &= E(|x'_{*,i} - x'_i(0)|) \\ &= E(x'_{*,i} - x'_i(0)|x'_{*,i} = x^+_i > 0)\mathbf{Pr}(x'_{*,i} = x^+_i) \\ &\quad + E(x'_{*,i} + x'_i(0)|x'_{*,i} = x^-_i < 0)\mathbf{Pr}(x'_{*,i} = x^-_i) \\ &= E(x'_{*,i}) - x'_i(0)\mathbf{Pr}(x'_{*,i} = x^+_i) + x'_i(0)\mathbf{Pr}(x'_{*,i} = x^-_i) \\ &= E(x'_{*,i}) - \frac{1}{2}x'_i(0) + \frac{1}{2}x'_i(0) \\ &= E(x'_{*,i}), \end{aligned} \quad (91)$$

which is the expected value of $E(|x_{*,i} - x_i(0)|)$ when $\mathbf{x}(0) = 0$. We will therefore assume for the remainder of this proof that $\mathbf{x}(0) = \mathbf{z}(0) = 0$.

Consider the motion along one axis. Let ξ_k^i, for $i = 1, 2$, denote the the values of $\xi_{i,j}^i$ along the i^{th} axis; so that $\xi_k^1 = \xi_{k,0}^1$ and $\xi_k^2 = \xi_{0,k}^2$. As in the one-dimensional case, we can write:

$$E(|x_*^i|) = \frac{1}{2}\int_{-\infty}^{\infty} |x^i|\rho_{|x_*^i|}(x^i|\xi_0^i > 0)\mathrm{d}x^i + \frac{1}{2}\int_{-\infty}^{\infty} |x^i|\rho_{|x_*^i|}(x^i|\xi_0^i < 0)\mathrm{d}x^i. \tag{92}$$

This case differs from the one-dimensional case, however, in that claims III.1 and III.2 no longer hold, since the particle is moving in two dimensions, and may therefore circumvent the region of positive (or negative) flow around $x^i = 0$ by moving along the perpendicular directions.

It follows from the symmetry of ρ_ξ that $\int_{-\infty}^{\infty} |x^i|\rho_{|x_*^i|}(x^i|\xi_0^i > 0)\mathrm{d}x^i = \int_{-\infty}^{\infty} |x^i|\rho_{|x_*^i|}(x^i|\xi_0^i < 0)\mathrm{d}x^i$. Using this, we can write:

$$E(|x_*^i|) = \int_{-\infty}^{\infty} |x^i|\rho_{|x_*^i|}(x^i|\xi_0^i > 0)\mathrm{d}x^i. \tag{93}$$

Note that $x_*^i = \mathrm{argmin}_{x_+^i, x_-^i}\{|x|\}$, therefore $E(|x_*^i|)$ can be written as

$$\begin{aligned}
E(|x_*^i|) &= \sum_{k=0}^{\infty}\int_{-(k+1)h}^{-kh} |x^i|\rho_{|x_*^i|}(x^i|\xi_0^i > 0, \mathrm{d}1)\mathbf{Pr}(\mathrm{d}1|\xi_0^i > 0)\mathrm{d}x^i \\
&\quad + \sum_{k=0}^{\infty}\int_{x_k^i}^{x_k^i+h} |x^i|\rho_{|x_*^i|}(x^i|\xi_0^i > 0, \mathrm{d}2)\mathbf{Pr}(\mathrm{d}2|\xi_0^i > 0)\mathrm{d}x^i \\
&= \sum_{k=0}^{\infty}\int_{-kh}^{-(k+1)h} x^i\rho_{|x_*^i|}(x^i|\xi_0^i > 0, \mathrm{d}1)\mathbf{Pr}(\mathrm{d}1|\xi_0^i > 0)\mathrm{d}x^i \\
&\quad + \sum_{k=0}^{\infty}\int_{x_k^i}^{x_k^i+h} x^i\rho_{|x_*^i|}(x^i|\xi_0^i > 0, \mathrm{d}2)\mathbf{Pr}(\mathrm{d}2|\xi_0^i > 0)\mathrm{d}x^i
\end{aligned} \tag{94}$$

where we have adopted the shorthand $\mathrm{d}1$ for the condition "$x_* = x_-^i, x_-^i \in (-(k+1)h, -kh)$" and $\mathrm{d}2$ for "$x_* = x_+^i, x_+^i \in (kh, (k+1)h)$", for notational convenience.

Using Lemmas III.6 and III.7, and applying change of variables

$$\begin{aligned}
u &= x - \left\lfloor \frac{x}{h} \right\rfloor h \\
v &= \xi^i_{\left\lfloor \frac{x}{h} \right\rfloor}
\end{aligned} \tag{95}$$

we can write (94) as

$$\begin{aligned}
&E(|x_*^i|) = \\
&\sum_{k=0}^{\infty} \Bigg\{ \frac{k}{4^{k+1}} \int_{-kh}^{-(k+1)h} x^i \rho_{|x_*^i|}(x^i|\xi_0^i > 0, \mathrm{d}1)\mathrm{d}x^i \\
&+ \frac{k}{4^{k+1}} \int_{-kh}^{-(k+1)h} x^i \rho_{|x_*^i|}(x^i|\xi_0^i > 0, \mathrm{d}1) \\
&\qquad \times \left[1 - \int_0^{|x^i|-kh} \frac{4h}{u^2} \left(\int_0^{\infty} v \rho_\xi(v) \rho_\xi(v(1-h/u)) \mathrm{d}v \right) \mathrm{d}u \right] \mathrm{d}x^i \\
&+ \frac{k+2}{4^{k+1}} \int_{kh}^{(k+1)h} x^i \rho_{|x_*^i|}(x^i|\xi_0^i > 0, \mathrm{d}2)\mathrm{d}x^i \\
&+ \frac{k}{4^{k+1}} \int_{kh}^{(k+1)h} x^i \rho_{|x_*^i|}(x^i|\xi_0^i > 0, \mathrm{d}2) \\
&\qquad \times \left[1 - \int_0^{x^i-kh} \frac{4h}{u^2} \left(\int_0^{\infty} v \rho_\xi(v) \rho_\xi(v(1-h/u)) \mathrm{d}v \right) \mathrm{d}u \right] \mathrm{d}x^i \Bigg\}.
\end{aligned} \tag{96}$$

Using the symmetry of ρ_ξ, we can combine terms in the above equation to obtain:

$$\begin{aligned}
E(|x_*^i|) = \sum_{k=0}^{\infty} \Bigg\{ & \frac{2(k+1)h}{4^{k+1}} \int_{-kh}^{-(k+1)h} x^i \rho_{|x_*^i|}(x^i|\xi_0^i > 0, \mathrm{d}1)\mathrm{d}x^i \\
& + \frac{2k}{4^{k+1}} \int_{-kh}^{-(k+1)h} x^i \rho_{|x_*^i|}(x^i|\xi_0^i > 0, \mathrm{d}1) \\
& \times \left[1 - \int_0^{|x^i|-kh} \frac{4h}{u^2} \left(\int_0^{\infty} v \rho_\xi(v) \rho_\xi(v(1-h/u)) \mathrm{d}v \right) \mathrm{d}u \right] \mathrm{d}x^i \Bigg\}
\end{aligned} \tag{97}$$

Substituting in the pdf derived in (40), we get:

$$\begin{aligned}
E(|x_*^i|) = \sum_{k=0}^{\infty} \Bigg\{ & \frac{2(k+1)h}{4^{k+1}} \int_{-kh}^{-(k+1)h} \int_0^{\infty} \frac{4hv}{x^i} \rho_\xi(v) \rho_\xi(v(1-h/x^i)) \mathrm{d}v \mathrm{d}x^i \\
& + \frac{2k}{4^{k+1}} \int_{-kh}^{-(k+1)h} \int_0^{\infty} \frac{4hv}{x^i} \rho_\xi(v) \rho_\xi(v(1-h/x^i)) \\
& \times \left[1 - \int_0^{|x^i|-kh} \int_0^{\infty} \frac{4hv}{u^2} \rho_\xi(v) \rho_\xi(v(1-h/u)) \mathrm{d}v \mathrm{d}u \right] \mathrm{d}v \mathrm{d}x^i \Bigg\}.
\end{aligned} \tag{98}$$

The above expression holds for $i = 1, 2$, so $E(|\mathbf{x}_*|_1) = E(|x_*^1| + |x_*^2|) = E(|x_*^1|) + E(|x_*^2|) = 2E(|x_*^i|)$. This proves Theorem III.1 in the general case. If ξ has a Gaussian distribution, the above expression may be evaluated numerically to give

$$E(|x_*^i|) = 1.26h, \tag{99}$$

from which it follows that, in this case, $E(|\mathbf{x}_*|) = 2.52h$. This completes the proof of Theorem III.1. ■

We have shown the expected value of the ℓ^1 norm of the position estimation error in the 2-D case. This gives a range on the expected value of the ℓ^2 error as follows:

$$\| \chi \|_1 / \sqrt{2} \leq \| \chi \|_2 \leq \| \chi \|_1 \tag{100}$$

for all $\chi \in \mathbb{R}^2$. Therefore we can say that in the case that ξ are Gaussian random variables, the expected value of the ℓ^2 norm of the position estimation error satisfies:

$$E(\| \mathbf{x}_* \|_2) \in [1.78h, 2.52h]. \tag{101}$$

Note that the above calculations do not depend on the strength of the error flow values at the gridpoints, only on the fact that they are independent, identically distributed random variables. The strength (that is, the variance) of the flow, however, does affect the time it takes for the error growth to reach an equilibrium. Since the velocity of the particle in the ocean flow is given by a bilinear interpolation of the flow values at the gridpoints, the higher the variance of the gridpoint values, the higher the mean velocity; and consequently, the faster the particles converge to an equilibrium of the error flow field.

The above approach does not address the coupling between the x and y-position of the expected equilibrium. This coupling is due to the bilinear interpolation of the gridpoint flow values. Because it is a bilinear interpolation of gridpoint values, the error flow along each of the x and y directions is a continuous function in $\mathbb{R}^2$, with continuous curves marking its level sets; in particular, the curves $\mathbf{f}^1(\mathbf{x}) = 0$ and $\mathbf{f}^2(\mathbf{x}) = 0$ are continuous curves (see Fig. 1). The average distance to the nearest equilibrium, therefore, depends not only on the average distance to an equilibrium along a particular axis, but also on the shape of the zero-level set curve. This can be understood via the following simple example: consider two lines $y = 0$ and $y = h$, with zero-crossings at $x = 1$ and $x = -2$, respectively. The sample mean of the norms of the crossing values is $(|1| + |-2|)/2 = 1.5$. Consider a straight line joining the two crossing points. The mean distance from the y-axis to this line is $5/6h$. In general, the distance to the zero level set curve along the x and y-directions is less than the expected distance to an equilibrium along a particular line parallel that axis; for this reason, Theorem III.1 gives an upper bound on the true value of $E_f(\| \mathbf{x}_* \|_1)$ at steady state.

IV. Eddy Diffusivity Contribution to CLPT Error Growth

The random-flight model (2) is frequently used to model motions of fluid particles in homogeneous, isotropic turbulence. In our model, we assume that the controlled particle is likewise subject to motion due to small-scale turbulent flows; in this section we consider the contribution of these turbulence-induced motions on the growth of the CLPT error.

We reproduce here the Langevin equation governing the dynamics of the controlled particle:

$$\mathrm{d}\mathbf{x} = (\mathbf{F}(\mathbf{x},t) + \mathbf{u}(\mathbf{x},t) + \nu)\,\mathrm{d}t \tag{102}$$

$$\mathrm{d}\nu = -A\nu\mathrm{d}t + \Lambda\mathrm{d}\omega \tag{103}$$

Under assumption (A1), $\mathbf{u}(\mathbf{x},t)$ has been chosen to cancel the estimated flow $\hat{\mathbf{F}}(\mathbf{x},t) = \mathbf{F}(\mathbf{x},t) + \mathbf{f}(\mathbf{x},t)$. For simplicity, we further assume that the spin parameter Ω in (3) may be ignored, so that $A = \frac{1}{\tau}I$ and $\Lambda = \sigma\sqrt{\frac{2}{\tau}}I$, where I is the identity matrix in $\mathbb{R}^2$. To simplify the notation, we define $a = 1/\tau$ and $L = \sigma\sqrt{\frac{2}{\tau}}$. Let $\mathbf{q}$ denote the particle state, $[\mathbf{x},\, \nu]^T$. The total equation for the evolution of $\mathbf{q}$ can be written in standard Ito form as

$$\mathrm{d}\mathbf{q} = \begin{bmatrix} 0 & I \\ 0 & -A \end{bmatrix}\mathbf{q} + \begin{bmatrix} 0 & 0 \\ 0 & \Lambda \end{bmatrix}(\hat{\mathbf{e}}_3\mathrm{d}\omega_1 + \hat{\mathbf{e}}_4\mathrm{d}\omega_2) \tag{104}$$

where $\hat{\mathbf{e}}_i$, $i = 1,\ldots,4$, are standard basis vectors in $\mathbb{R}^4$, and the initial position of the particle, $\mathbf{x}(t_0)$, is assumed to be 0.

Claim IV.1. *The CLPT error growth due to the stochastic velocity term ν, for the case that $\mathbf{f} \equiv 0$, satisfies:*

$$\| \mathbf{e}_\nu(t) \| \leq \sqrt{\frac{2L}{a^2}}t^{\frac{1}{2}}. \tag{105}$$

when $t > \tau$.

To complete the proof of this claim, we need the following two Lemmas:

Lemma IV.1. *Let $\psi_2 = \nu^{\mathrm{T}}\nu$, and say $\nu(0) = 0$, so that $\psi_2(0) = 0$. Then,*

$$E\left(\psi_2(t)\right) = \frac{L}{a}\left(1 - e^{-2at}\right). \tag{106}$$

Proof: ψ_2 can be expressed as

$$\psi_2 = \mathbf{q}^{\mathrm{T}}\begin{bmatrix} 0 & 0 \\ 0 & I \end{bmatrix}\mathbf{q}. \tag{107}$$

Using this definition,it can be easily shown that

$$\frac{\mathrm{d}E\left(\psi_2(t)\right)}{\mathrm{d}t} = -2aE\left(\psi_2\right) + 2L. \tag{108}$$

This is a standard first-order ODE with solution given by

$$E\left(\psi_2(t)\right) = \frac{L}{a}\left(1 - e^{-2at}\right). \tag{109}$$

This proves the Lemma. ■

Lemma IV.2. *Let* $\psi_1 = \mathbf{x}^{\mathrm{T}}\nu$*, and say* $\mathbf{x}(0) = \nu(0) = 0$*, so that* $\psi_1(0) = 0$*. Then,*

$$E\left(\psi_1(t)\right) = \frac{L}{a^2} - \frac{2L}{a^2}e^{-at} + \frac{L}{a^2}e^{-2at}. \tag{110}$$

Proof: Given

$$\psi_1 = \mathbf{x}^{\mathrm{T}}\nu = \mathbf{q}^{\mathrm{T}}\begin{bmatrix} 0 & I \\ 0 & 0 \end{bmatrix}\mathbf{q}, \tag{111}$$

it is easy to show that

$$\frac{\mathrm{d}E\left(\psi_1(t)\right)}{\mathrm{d}t} = -aE\left(\psi_1(t)\right) + E\left(\psi_2(t)\right). \tag{112}$$

Using Lemma IV.1:

$$\frac{\mathrm{d}E\left(\psi_1(t)\right)}{\mathrm{d}t} = -aE\left(\psi_1(t)\right) + \frac{L}{a}\left(1 - e^{-2at}\right). \tag{113}$$

This is a non-homogeneous linear ODE, which we solve explicitly to get:

$$E\left(\psi_1(t)\right) = e^{-at}\int_0^{\mathrm{T}} e^{as}\frac{L}{2a}\left(1 - e^{-2as}\right)\mathrm{d}s \tag{114}$$

$$= \frac{L}{a^2} - \frac{2L}{a^2}e^{-at} + \frac{L}{a^2}e^{-2at}. \tag{115}$$

This proves the Lemma. ■

We now proceed to the proof of Claim IV.1:

Proof: Given perfect mean flow cancellation, and $\mathbf{f} \equiv 0$ (that is, $\hat{\mathbf{F}} = \mathbf{F}$), (4) gives $\mathbf{z}(t) = 0$, thus $\mathbf{z}(t) = \mathbf{z}(0) = 0$. The CLPT error is then given by

$$e(t) = \|\,\mathbf{x}(t) - \mathbf{z}(t)\,\| = \|\,\mathbf{x}(t)\,\|, \tag{116}$$

with dynamics of $\mathbf{x}$ given by (104), where $\|\cdot\|$ is the standard ℓ^2-norm in $\mathbb{R}^4$. We define ψ as the square of the CLPT error,

$$\psi = e^2 = \|\,\mathbf{x}(t)\,\|^2 = \mathbf{q}^{\mathrm{T}}\begin{bmatrix} I & 0 \\ 0 & 0 \end{bmatrix}\mathbf{q}. \tag{117}$$

It is easy to show that:

$$\frac{\mathrm{d}E(\psi)}{\mathrm{d}t} = 2E\left(\mathbf{q}^{\mathrm{T}}\begin{bmatrix} 0 & I \\ 0 & 0 \end{bmatrix}\mathbf{q}\right) = 2E\left(\mathbf{x}^{\mathrm{T}}\nu\right) = 2E\left(\psi_1\right). \tag{118}$$

Then by lemma IV.2,

$$\frac{\mathrm{d}E\left(\psi(t)\right)}{\mathrm{d}t} = \frac{2L}{a^2} - \frac{4L}{a^2}e^{-at} + \frac{2L}{a^2}e^{-2at}. \tag{119}$$

This equation can be directly integrated (given $\psi(0) = 0$) to find

$$E\left(\psi(t)\right) = \frac{2L}{a^2}t + \frac{4L}{a^3}e^{-at} - \frac{L}{a^3}e^{-2at} - \frac{3L}{a^3}, \tag{120}$$

which is bounded above by $\frac{2L}{a^2}t$ for $t > 1/a = \tau$, the Lagrangian correlation time of the system.

The expected value of $\| \mathbf{e}_\nu(t) \| = \| \mathbf{x}(t) \|$ can be restricted by Jensen's inequality:

$$E\left(\| \mathbf{x}(t) \|\right) = E\left(\sqrt{\psi(t)}\right) \leq \sqrt{E\left(\psi(t)\right)} < \alpha t^{\frac{1}{2}} \tag{121}$$

with $\alpha = \sqrt{\frac{2L}{a^2}}$, for t larger than the correlation time scales of the system. Thus, positioning error growth due to the stochastic eddy diffusivity term is bounded above by a square-root time growth law. ■

Remarks: We can now combine the results of sections III and IV to summarize the characteristics of the growth of CLPT error. The initial error growth is dominated by the error contributions due to large-scale error flow $\mathbf{f}$, which represents inaccuracies in the model prediction of the mean flow field. This causes an initially exponential CLPT error growth; however, this contribution to the error growth becomes small when the particle reaches an equilibrium of the error flow field. The long-term error contribution is dominated by the eddy diffusivity ν, with CLPT error growth on the order of $t^{1/2}$, justified by Claim IV.1.

V. Simulation and the ASAP Field Experiment

In deriving the upper threshold for exponential CLPT error growth between simulated particles and particles moving in real ocean environments, we have made several simplifying assumptions about the structure of the error field. To demonstrate that the results hold in more complicated situations, we compare them with simulation and observations made during the 2006 ASAP experiment.

A. Simulation of CLPT Error Growth

The CLPT error results are first tested in simulation. We design two simulations: the first, to verify the expected values for CLPT error due to modeling flow error $\mathbf{f}$; the second, to demonstrate motion of controlled agents in the flow defined by (13).

In the first simulation, we select a square area of interest, centered at the origin, and cover it with a grid whose gridsize is normalized to $h = 1$. We simulate the error flow $\mathbf{f}$ by assigning Gaussian-distributed random flow values (with diagonal covariance matrix) at each gridpoint. Using these values, we then solve for all equilibrium points, where $\mathbf{f} = 0$. In the 1-D case, equilibria are kept only if they correspond to a stable equilibrium, i.e., if $\frac{\mathrm{d}f}{\mathrm{d}x} < 0$. In the 2-D case, equilibria are kept if they satisfy the necessary stability criteria, $\frac{\partial f^1}{\partial x} < 0$ and $\frac{\partial f^2}{\partial y} < 0$. Given the set of equilibria z_{eq}, we record:

$$|z_*|_1 = \min_{z_{eq}} \left(|z|_1 \right). \tag{122}$$

The above calculation is repeated 10^5 times for each of the 1-D and 2-D cases, and the sample mean taken over all runs. This gives a sample mean of the ℓ^1-norm to the nearest equilibrium that satisfies necessary stability conditions in the 1-D and 2-D cases.

In the 1-D case, the sample mean of the distance to the equilibrium is 1.5, which agrees with the theoretical value of $1.5h$ calculated in Section III. In the 2-dim case, the sample mean of the minimum 1-norm of the equilibrium is $1.92h$. This is less than $2.52h$, the expected value of the 1-norm of the error computed in Section III, which agrees with Theorem III.1.

The second simulation demonstrates how the results for position estimation error growth are affected by small-scale turbulent flow, modeled by the ν term in the Langevin equation (11). In this simulation, we again set up a 2-D region of interest, centered at the origin, and cover it with a grid. The gridsize used is 0.9 km and 1.8 km (the latter value, 1.8 km was chosen to correspond to the gridsize used by the ROMS ocean model in the physical glider deployment in Monterey Bay; see Section V-B). The values of the error flow $\mathbf{f}$ at gridpoints are normally distributed random variables with diagonal covariance matrix (given by $\sigma_{\mathbf{f}}\mathbf{I}_{2\times 2}$). Flow values at the particle position are obtained using bilinear interpolation of the gridpoint values, with added stochastic drift ν. An Euler-Maruyama integrator is used to find particle positions over time. The simulation is run with 1000 repetitions, for different values of the variance σ_ν (the variance of driving noise in ν), $1/\tau$, and $\sigma_{\mathbf{f}}$. Fig. 2 shows the average ℓ^2-norm of the particle position over

time for different values of the simulation parameters. The error growth is initially dominated by the error due to the error flow $\mathbf{f}$; for longer times, the error is dominated by the small-scale stochastic terms. The shape of the error growth curve depends on the relative strengths of these two contributions, as shown in Fig. 2.

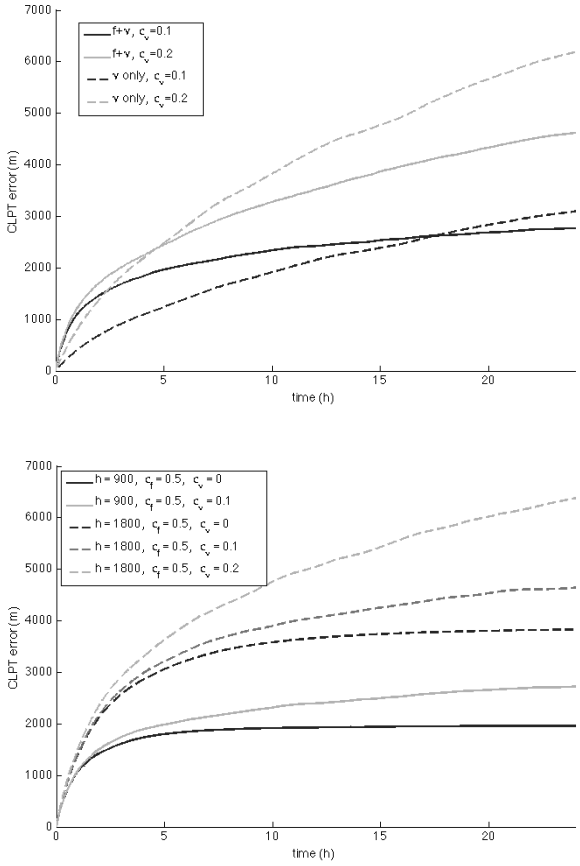

Fig. 2. (Top) Comparison of CLPT error growth with and without model error flow $\mathbf{f}$. The dotted lines show simulated error growth in the case $\mathbf{f} \equiv 0$; solid lines show simulated error growth with $\sigma_{\mathbf{f}} = 0.5$ for an ocean model with gridsize $h = 0.9$ km. The Lagrangian correlation time is $\tau = 1$ hr. (Bottom) CLPT error growth over time for varying ocean model gridsize and σ_ν. The variance of ocean model flow values at gridpoints is $\sigma_{\mathbf{f}} = 0.5$. The Langevin correlation time is 1 hr.

B. ASAP Field Experiment Results

The CLPT theoretical results were inspired by observations made during the Adaptive Sampling and Prediction (ASAP) field experiment in Monterey Bay, CA, in August 2006. We now apply the theoretical CLPT results to explain observed errors in simulating positions of

autonomous underwater gliders during the experiment. We note that gliders are hardly ideal Lagrangian particles; they have finite mass and volume, and a complex coupling exists between the glider motion and surrounding flow. Moreover, gliders move in a 3-dimensional time-varying flow. However, in this section we consider only the horizontal component of glider motion, using depth-averaged flow velocity for the 2-dimensional flow field used in our CLPT analysis. We show that the characteristic shape of the CLPT error growth may be observed, in spite of the non-Lagrangian nature of the physical gliders.

The scientific goal of the experiment was to study the three-dimensional heat and mass transfer dynamics of the coastal upwelling center of Monterey Bay [27], [46]. A heterogeneous glider sensor network was used to continuously monitor a 20×40 km control volume over a period of one month. The sensor array included a fleet of 6 Slocum underwater gliders [27]. The glider tracks were selected to optimize an adaptive sampling metric (see [26] for details).

The Slocum gliders use Iridium satellite telephones for bidirectional communication with an on-shore server. The glider trajectories are specified by waypoint lists passed to each glider via the server. The glider then follows the specified trajectory using an onboard controller.

It should be noted that Slocum gliders have an option for current correction; using this option enables an on-board flow cancellation algorithm. The glider maintains an on-board estimate of the depth-averaged current over the previous dive. When operating with current correction, the glider adjusts its heading to cancel the on-board flow estimate based on surfacing data collected for the previous dive. In coastal environments with tidal flows that change significantly over the dive time of the glider, this flow-canceling algorithm generally performs poorly; during the ASAP experiment, the on-board current correction was therefore turned off.

The waypoints were generated using an onshore computer connected via network with the glider server. The implementation was done using the Glider Coordinated Control System (GCCS), a Matlab-based glider control software written at Princeton by D. Paley and F. Zhang. A detailed description of the GCCS is given in [38], [47]. GCCS consists of three modules: a simulation module, a planning module, and a communication module used to transmit data between GCCS and the glider server. The planning module uses a detailed 3-dimensional glider model, together with estimated flow data, to predict future glider surfacings. A faster, less accurate glider model is then used to generate desired trajectories based on the predicted surfacing positions, and to convert these to waypoint lists. When a glider surfaces, the communication module is used to

send the waypoint list for that glider; the glider's surfacing position is used to initialize the simulation to predict the surfacing position for the next dive. GCCS can also be run in simulator mode; in this case, the gliders and glider server are replaced with the GCCS simulator module for testing and controller verification purposes.

The controller used in the ASAP experiment was designed to coordinate the motions of the gliders along their desired trajectories, while maintaining optimal spacing for good sampling performance. A detailed description of the controller used is given in [48], [47]. Note that this controller assumes zero flow conditions; the controller applied, then, used a superposition of a flow-canceling control and a the coordinated controller. The flow to be canceled was estimated as a weighted average of glider onboard flow estimates.

A virtual glider experiment was run alongside the physical experiment, using the GCCS simulation node. The gliders in the virtual fleet were modeled using true glider parameters, and the same proprietary on-board controller as that used by the physical gliders. The virtual gliders were initialized at the same positions as their physical counterparts, and their motions were simulated using flow data from ocean models. The experiment was repeated for three different models: the Navy Coastal Ocean Model/Innovative Coastal Ocean Observing Network (NCOM/ICON) [49], the Harvard Ocean Prediction System (HOPS, http://modelseas.mit.edu/HOPS/) [50], and the Regional Ocean Modeling System (ROMS, http://www.myroms.com) [51] developed by NASA JPL. The NCOM model is a free-surface, primitive-equation model with global global temperature and salinity data assimilation from the Modular Ocean Data Assimilation System (MODAS). The model is discretized on a grid with resolution o approximately 2.24 km over the study site, and provides a 72-hour flow forecast. The HOPS model is a primitive equation model adapted for coastal applications. The ROMS model is a free-surface, terrain-following, primitive equation model with mean gridsize of $1.8 - 2.2$ km over the study domain. The flow values at the glider position for each ocean model were obtained using a linear interpolation of the model flow gridpoint values. Each virtual experiment was run over a period of 24 hours.

A plot of the norm of the error in the position prediction over time (averaged over all gliders and all days for which data is available) obtained using the virtual glider model is shown in Fig. 3. This figure was generated by measuring the separation (CLPT error) between the physical gliders and their simulated counterparts for each ocean model at surfacing positions, and taking the linear interpolation of this error to $1/2$-hour intervals; the separation values at each time

were then averaged over each of the gliders in the fleet, and over all days of the simulation. The figure is overlaid with plot of CLPT error growth simulated using the Langevin equation with ocean model gridsize of 1.8 km, stochastic forcing with $\sigma_\nu = 0.05$ and 0.07, and error flow at gridpoints with variance of 0.2, averaged over 1000 runs. Note that the error grows approximately exponentially until a value of about twice the gridsize is reached; past this point, the growth rate slows down. This agrees with the CLPT prediction of the upper threshold for exponential growth of the CLPT error, and with the contribution of the stochastic eddy diffusivity term in the Langevin equation.

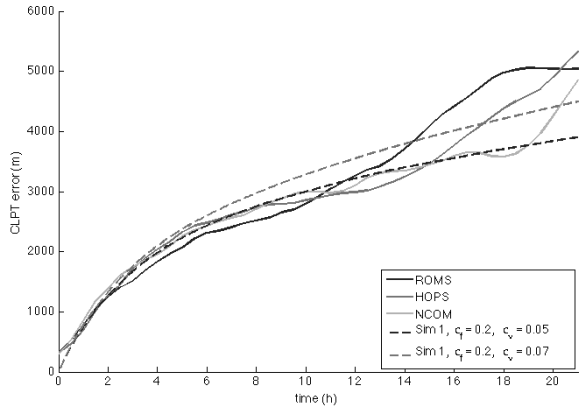

Fig. 3. CLPT error growth observed in the ASAP experiment, averaged over all gliders and all runs. The CLPT error is the magnitude of the error in position estimation obtained using an ocean model. The solid lines are plots of mean CLPT error (averaged over all gliders and all days of the simulation) are shown for each of the three ocean models used in the experiment. The dashed lines show CLPT error simulated using the Langevin equation with drift given by error flow $\mathbf{f}$, with model error flow variance 0.2, and $\sigma_\nu = 0.05$ and 0.07, respectively. The simulations were run with gridsize of 1.8 km, which corresponds to the gridsize used by the ROMS ocean model in the ASAP field experiment. The simulated CLPT error growth results give good qualitative agreement with the observed experimental data.

VI. Conclusion and future work

This paper develops the theory of controlled Lagrangian particle tracking (CLPT). In particular, we theoretically justified the observations made through experiments that the CLPT error has slower growth rate than the LPT error. We have discovered that the CLPT error growth is initially exponential, but slows to polynomial growth when the error crosses a threshold that is determined by the gridsize of the ocean model that is used for making position predictions.

In our treatment of the CLPT error, we have assumed a particularly simple structure for the error flow in order to make our calculations tractable. This error flow is, in reality, very difficult to characterize. In future work, we propose to incorporate observations of glider position (made at surfacing times) to update the model flow and to create a model-based observer for the positions of actuated agents. This approach will be used to obtain more accurate positioning of the underwater vehicles, as well as to study the true structure of the error flow.

ACKNOWLEDGEMENTS

We would like to thanks the HOPS team, the NRL NCOM team and the JPL ROMS team for providing ocean models.

REFERENCES

[1] A. J. Mariano, A. Griffa, T. M. Özgökmen, and E. Zambianchi, "Lagrangian analysis and predictability of coastal and ocean dynamics 2000," *Journal of Atmospheric and Oceanic Technology*, vol. 19, no. 7, pp. 1114–1126, 2002.

[2] H. Salman, L. Kuznetsov, C. K. R. T. Jones, and K. Ide, "A method for assimilating Lagrangian data into a shallow-water-equation ocean model," *Monthly Weather Review*, vol. 134, pp. 1081–1101, Apr. 2006.

[3] M. Gomez-Gesteira, P. Montero, R. Prego, J. J. Taboada, P. Leitao, M. Ruiz-Villarreal, R. Neves, and V. Perez-Villar, "A two-dimensional particle tracking model for pollution dispersion in A Coruña and Vigo Rias (NW Spain)," *Oceanologica Acta*, vol. 22, pp. 167–177, Mar. 1999.

[4] A. Lugo-Fernandez, K. J. P. Deslarzes, J. M. Price, G. S. Boland, and M. V. Morin, "Inferring probable dispersal of Flower Garden Banks Coral Larvae (Gulf of Mexico) using observed and simulated drifter trajectories," *Continental Shelf Research*, vol. 21, no. 1, pp. 47–67, 2001.

[5] E. Staaterman, C. B. Paris, and J. Helgers, "Orientation behavior in fish larvae: a missing piece to Hjort's critical period hypothesis.," *Journal of theoretical biology*, vol. 304, pp. 188–96, July 2012.

[6] M. Cerejo and J. M. Dias, "Tidal transport and dispersal of marine toxic microalgae in a shallow, temperate coastal lagoon," *Marine environmental research*, vol. 63, pp. 313–40, May 2007.

[7] H. Havens, M. E. Luther, S. D. Meyers, and C. A. Heil, "Lagrangian particle tracking of a toxic dinoflagellate bloom within the Tampa Bay estuary," *Marine pollution bulletin*, vol. 60, pp. 2233–41, Dec. 2010.

[8] G. I. Taylor, "Diffusion by continuous movements," *Proceedings of the London Mathematical Society*, vol. 20, pp. 373—-416, Jan. 1921.

[9] F. B. Smith, "Conditioned particle motion in a homogeneous turbulent field," *Atmospheric Environment*, vol. 2, no. 5, pp. 491–508, 1968.

[10] H. van Dop, F. T. M. Nieuwstadt, and J. C. R. Hunt, "Random walk models for particle displacements in inhomogeneous unsteady turbulent flows," *Physics of Fluids*, vol. 28, no. 6, pp. 1639–1653, 1985.

[11] D. J. Thomson, "A random walk model of dispersion in turbulent flows and its application to dispersion in a valley," *Quarterly Journal of the Royal Meteorological Society*, vol. 112, pp. 511–530, Apr. 1986.

[12] A. Griffa, "Applications of stochastic particle models to oceanographic problems," in *Stochastic Modeling in Physical Oceanography* (R. J. Adler, P. Müller, and B. Rozovskii, eds.), pp. 113–140, Boston: Birkhäuser, 1996.

[13] R. E. Davis, "Observing the general circulation with floats," *Deep Sea Research Part A Oceanographic Research*, vol. 38, no. Supplemental 1, pp. S531–S571, 1991.

[14] W. B. Owens, "A statistical description of the mean circulation and eddy variability in the northwestern Atlantic using SOFAR floats," *Progress in Oceanography*, vol. 28, no. 3, pp. 257–303, 1991.

[15] P. Richardson, "Drifters and floats," in *Encyclopedia Ocean Studies*, pp. 767–774, Academic Press Ltd., 2001.

[16] H.-M. Zhang, M. D. Prater, and T. Rossby, "Isopycnal Lagrangian statistics from the North Atlantic Current RAFOS float observations," *Journal of Geophysical Research*, vol. 106, no. C7, pp. 13817–13836, 2001.

[17] T. M. Özgökmen, A. Griffa, A. J. Mariano, and L. I. Piterbarg, "On the predictability of Lagrangian trajectories in the ocean," *Journal of Atmospheric and Oceanic Technology*, vol. 17, pp. 366–383, Mar. 2000.

[18] H. Salman, K. Ide, and C. K. R. T. Jones, "Using flow geometry for drifter deployment in Lagrangian data assimilation," *Tellus A*, vol. 60, pp. 321–335, Mar. 2008.

[19] A. Griffa, L. I. Piterbarg, and T. M. Özgökmen, "Predictability of Lagrangian particle trajectories: effects of smoothing of the underlying Eulerian flow," *Journal of Marine Research*, vol. 62, pp. 1–35, Jan. 2004.

[20] E. Ferreira-Coelho and M. Rixen, "Maritime rapid environmental assessment new trends in operational oceanography," *Journal of Marine Systems*, vol. 69, pp. 1–2, Jan. 2008.

[21] M. Rixen, E. Ferreira-Coelho, and R. Signell, "Surface drift prediction in the Adriatic Sea using hyper-ensemble statistics on atmospheric, ocean and wave models: uncertainties and probability distribution areas," *Journal of Marine Systems*, vol. 69, pp. 86–98, Jan. 2008.

[22] L. Kuznetsov, K. Ide, and C. K. R. T. Jones, "A method for assimilation of lagrangian data," *Monthly Weather Review*, vol. 131, pp. 2247–2260, Dec. 2003.

[23] D. L. Rudnick, R. E. Davis, C. C. Eriksen, D. M. Fratantoni, and M. J. Perry, "Underwater gliders for ocean research," *Marine Technology Society Journal*, vol. 38, pp. 73–84, June 2004.

[24] L. L. Whitcomb, D. Yoerger, H. Singh, and J. Howland, "Advances in underwater robot vehicles for deep ocean exploration: navigation, control, and survey operations," in *Proceedings Ninth International Symposium of Robotics Research*, pp. 346–353, 1999.

[25] T. B. Curtin, J. G. Bellingham, J. Catipovic, and D. Webb, "Autonomous oceanographic sampling networks," *Oceanography*, vol. 6, no. 3, pp. 86–94, 1993.

[26] N. E. Leonard, D. A. Paley, F. Lekien, R. J. Sepulchre, D. M. Fratantoni, and R. E. Davis, "Collective motion, sensor networks, and ocean sampling," *Proceedings of the IEEE*, vol. 95, pp. 48–74, Jan. 2007.

[27] N. E. Leonard, D. A. Paley, R. E. Davis, D. M. Fratantoni, F. Lekien, and F. Zhang, "Coordinated control of an underwater glider fleet in an adaptive ocean sampling field experiment in Monterey Bay," *Journal of Field Robotics*, vol. 27, pp. 718–740, Nov. 2010.

[28] B. Garau, A. Alvarez, and G. Oliver, "Path planning of autonomous underwater vehicles in current fields with complex spatial variability: an A* approach," in *Proceedings of the 2005 IEEE International Conference on Robotics and Automation*, pp. 194–198, IEEE, 2005.

[29] B. Garau, M. Bonet, A. Alvarez, and S. Ruiz, "Path planning for autonomous underwater vehicles in realistic oceanic current fields: application to gliders in the western Mediterranean Sea," *Journal of Maritime Research*, vol. 6, no. 2, pp. 5–22, 2009.

[30] C. Pêtrès, Y. Pailhas, P. Patrón, Y. Petillot, J. Evans, and D. Lane, "Path planning for autonomous underwater vehicles," *IEEE Transactions on Robotics*, vol. 23, pp. 331–341, Apr. 2007.

[31] M. Soulignac, P. Taillibert, and M. Rueher, "Adapting the wavefront expansion in presence of strong currents," in *2008 IEEE International Conference on Robotics and Automation*, vol. 2008, pp. 1352–1358, IEEE, May 2008.

[32] M. Soulignac, P. Taillibert, and M. Rueher, "Time-minimal path planning in dynamic current fields," in *2009 IEEE International Conference on Robotics and Automation*, pp. 2473–2479, IEEE, May 2009.

[33] K. Sugihara and J. Yuh, "GA-based motion planning for underwater robotic vehicles," in *Proc. 10th International Symp. on Unmanned Untethered Submersible Technology*, pp. 406–415, 1996.

[34] J. C. Rubio and S. Kragelund, "The trans-pacific crossing: long range adaptive path planning for UAVs through variable wind fields," in *22nd Digital Avionics Systems Conference Proceedings (Cat No 03CH37449) DASC-03*, vol. 2, pp. 8.B.4–1–12, IEEE, 2003.

[35] A. Alvarez, A. Caiti, and R. Onken, "Evolutionary path planning for autonomous underwater vehicles in a variable ocean," *IEEE Journal of Oceanic Engineering*, vol. 29, no. 2, pp. 418–429, 2004.

[36] C. Vasudevan and K. Ganesan, "Case-based path planning for autonomous underwater vehicles," *Autonomous Robots*, vol. 3, no. 2-3, pp. 79–89, 1996.

[37] F. Zhang, D. M. Fratantoni, D. A. Paley, J. M. Lund, and N. E. Leonard, "Control of coordinated patterns for ocean sampling," *International Journal of Control*, vol. 80, pp. 1186–1199, July 2007.

[38] D. A. Paley, F. Zhang, and N. E. Leonard, "Cooperative control for ocean sampling: the Glider Coordinated Control System," *IEEE Transactions on Control Systems Technology*, vol. 16, pp. 735–744, July 2008.

[39] R. N. Smith, Y. Chao, P. P. Li, D. A. Caron, B. H. Jones, and G. S. Sukhatme, "Planning and implementing trajectories for autonomous underwater vehicles to track evolving ocean processes based on predictions from a regional ocean model," *The International Journal of Robotics Research*, vol. 29, pp. 1475–1497, Aug. 2010.

[40] F. S. Hover, "Path planning for data assimilation in mobile environmental monitoring systems," in *2009 IEEE/RSJ International Conference on Intelligent Robots and Systems*, pp. 213–218, Oct. 2009.

[41] N. K. Yilmaz, C. Evangelinos, P. Lermusiaux, and N. M. Patrikalakis, "Path planning of autonomous underwater vehicles for adaptive sampling using mixed integer linear programming," *IEEE Journal of Oceanic Engineering*, vol. 33, pp. 522–537, Oct. 2008.

[42] K. Szwaykowska and F. Zhang, "A lower bound for controlled Lagrangian particle tracking error," in *49th IEEE Conference on Decision and Control (CDC)*, pp. 4353–4358, Dec. 2010.

[43] K. Szwaykowska and F. Zhang, "A lower bound on navigation error for marine robots guided by ocean circulation models," in *2011 IEEE/RSJ International Conference on Intelligent Robots and Systems*, pp. 3583–3588, IEEE, Sept. 2011.

[44] A. C. Haza, L. I. Piterbarg, P. Martin, T. M. Özgökmen, and A. Griffa, "A Lagrangian subgridscale model for particle transport improvement and application in the Adriatic Sea using the Navy Coastal Ocean Model," *Ocean Modelling*, vol. 17, pp. 68–91, Jan. 2007.

[45] P. Falco, A. Griffa, P.-M. Poulain, and E. Zambianchi, "Transport properties in the Adriatic Sea as deduced from drifter data," *Journal of Physical Oceanography*, vol. 30, pp. 2055–2071, Aug. 2000.

[46] S. R. Ramp, R. E. Davis, N. E. Leonard, I. Shulman, Y. Chao, A. R. Robinson, J. E. Marsden, P. F. J. Lermusiaux, D. M. Fratantoni, J. D. Paduan, F. P. Chavez, F. L. Bahr, S. Liang, W. Leslie, and Z. Li, "Preparing to predict: the second autonomous ocean sampling network (AOSN-II) experiment in the Monterey Bay," *Deep Sea Research Part II: Topical Studies in Oceanography*, vol. 56, pp. 68–86, Feb. 2009.

[47] D. A. Paley, *Cooperative control of collective motion for ocean sampling with autonomous vehicles*. Phd thesis, Princeton University, 2007.

[48] D. A. Paley, N. E. Leonard, and R. J. Sepulchre, "Collective motion of self-propelled particles: Stabilizing symmetric formations on closed curves," in *Proc. of the 45th Conference on Decision and Control*, pp. 5067–5072, 2006.

[49] I. Shulman, C. R. Wu, J. K. Lewis, J. D. Paduan, L. K. Rosenfeld, J. C. Kindle, S. R. Ramp, and C. A. Collins, "High resolution modeling and data assimilation in the Monterey Bay area," *Continental Shelf Research*, vol. 22, pp. 1129–1151, May 2002.

[50] A. R. Robinson, "Forecasting and Simulating Coastal Ocean Processes and Variabilities with the Harvard Ocean Prediction System," in *Coastal Ocean Prediction* (C. N. K. Mooers, ed.), pp. 77–100, American Geophysical Union, 1999.

[51] A. F. Shchepetkin and J. C. McWilliams, "The regional oceanic modeling system (ROMS): a split-explicit, free-surface, topography-following-coordinate oceanic model," *Ocean Modelling*, vol. 9, pp. 347–404, Jan. 2005.

FIGURE CAPTIONS

1) Zero level set of the error flow in the x-direction, $\mathbf{f}^1(\mathbf{x}) = 0$. Equilibria of $\mathbf{f}(\mathbf{x})$ lie on intersections of the zero level sets for flow in the x- and y-directions.
2) (Top) Comparison of CLPT error growth with and without model error flow $\mathbf{f}$. The dotted lines show simulated error growth in the case $\mathbf{f} \equiv 0$; solid lines show simulated error growth with $\sigma_{\mathbf{f}} = 0.5$ for an ocean model with gridsize $h = 0.9$ km. The Lagrangian correlation time is $\tau = 1$ hr. (Bottom) CLPT error growth over time for varying ocean model gridsize and σ_ν. The variance of ocean model flow values at gridpoints is $\sigma_{\mathbf{f}} = 0.5$. The Langevin correlation time is 1 hr.
3) CLPT error growth observed in the ASAP experiment, averaged over all gliders and all runs. The CLPT error is the magnitude of the error in position estimation obtained using an ocean model. The solid lines are plots of mean CLPT error (averaged over all gliders and all days of the simulation) are shown for each of the three ocean models used in the experiment. The dashed lines are plots CLPT error simulated using the Langevin equation with drift given by error flow $\mathbf{f}$, with model error flow variance 0.2 and 0.3, respectively, and $\sigma_\nu = 0.1$. The simulations were run with gridsize of 1.8 km, which corresponds to the gridsize used by the ROMS ocean model in the ASAP field experiment. The simulated CLPT error growth results give good qualitative agreement with the observed experimental data.